Naval Research Laboratory

Washington, DC 20375-5320

NRL/MR/6685--99-8338

Plasma and X-UV Source Characteristics for Al Targets Heated by 40 Nsec Nd-laser Pulses

ROBERT R. WHITLOCK
DAVID J. NAGEL
STEPHEN J. TOPSCHER

Dynamics of Solids Branch
Condensed Matter and Radiation Sciences Division

J.R. GREIG

Mid Atlantic Radiation Physics, Inc.
Greenbelt, Maryland

March 16, 1999

REPORT DOCUMENTATION PAGE

Form Approved
OMB No. 0704-0188

1. AGENCY USE ONLY (*Leave Blank*)	2. REPORT DATE	3. REPORT TYPE AND DATES COVERED
	March 16, 1999	NRL Memorandum Report

4. TITLE AND SUBTITLE

Plasma and X-UV Source Characteristics for Al Targets Heated by 40 Nsec Nd-laser Pulses

5. FUNDING NUMBERS

66-2849-0-9

6. AUTHOR(S)

Robert R. Whitlock, J.R. Greig,* David J. Nagel, and Stephen J. Topscher

7. PERFORMING ORGANIZATION NAME(S) AND ADDRESS(ES)

Naval Research Laboratory
Washington, DC 20375-5320

8. PERFORMING ORGANIZATION REPORT NUMBER

NRL/MR/6685--99-8338

9. SPONSORING/MONITORING AGENCY NAME(S) AND ADDRESS(ES)

Office of Naval Research
Chief of Naval Research
Ballston Centre Tower One
800 North Quincy Street
Arlington, VA 22217-5660

10. SPONSORING/MONITORING AGENCY REPORT NUMBER

11. SUPPLEMENTARY NOTES

*Mid Atlantic Radiation Physics, Inc., 7233D Hanover Parkway, Greenbelt, MD 20770

12a. DISTRIBUTION/AVAILABILITY STATEMENT

Approved for public release; distribution unlimited.

12b. DISTRIBUTION CODE

13. ABSTRACT (*Maximum 200 words*)

The total laser energy (3-32 J), temporal history (40 nsec FWHM) and focal energy distribution (3×10^{13} W/cm^2 peak, 1.5×10^{13} W/cm^2 average) for $\lambda = 1.06$ μm Nd:glass laser interactions with planar Al targets were measured. Laser-produced plasma emissions within the 10 eV - 3 keV ultraviolet and x-ray range were recorded. Primary emphasis was given to obtaining the dependence of kilovolt x-ray emission on irradiance (varied by altering the energy on target or the lens-target spacing). A maximum efficiency for conversion of incident laser energy to radiation above 1.5 keV was 0.25% into 2π sr. Emitted x-ray intensity over this range of photon energy was found to increase as the 3.2 power of laser energy at best focus. X-ray emission decreased when a prepulse preceded the main pulse by a controlled amount exceeding 0.2 μs but <5 μs, with a minimum emission at 0.5 μs separation. Plasma temperatures were estimated from x-ray line intensity ratios and continuum slopes: a value near 230 eV was obtained from free-bound continuum slope for 3×10^{13} W/cm^2 peak irradiance. Temperatures decreased at lower irradiances, as inferred from x-ray line ratios.

This report covers systematic experimental measurements of laser plasma x-ray output. The work formed the basis for the later demonstration of microlithography with this same x-ray source, in support of the NRL patent for laser plasma x-ray lithography. The patent was licensed by a 100-person startup company, Hampshire Instruments, Inc., who offered a technically viable method to achieve submicron critical linewidths for the production of integrated circuits.

14. SUBJECT TERMS

Neodymium laser
Plasma
X-ray
Spectrum
Lithography

15. NUMBER OF PAGES

36

16. PRICE CODE

17. SECURITY CLASSIFICATION OF REPORT	18. SECURITY CLASSIFICATION OF THIS PAGE	19. SECURITY CLASSIFICATION OF ABSTRACT	20. LIMITATION OF ABSTRACT
UNCLASSIFIED	UNCLASSIFIED	UNCLASSIFIED	UL

NSN 7540-01-280-5500

Standard Form 298 (Rev. 2-89)
Prescribed by ANSI Std 239-18
298-102

CONTENTS

I. Introduction 1

II. Laser and Target Arrangement 2

III. Laser Beam Characteristics 4

IV. Broadband X-Ray Results 5

V. X-Ray Spectral Studies 8

VI. Effect of Prepulse on X-Ray Output 12

Conclusions 12

Acknowledgements 13

References 14

Table Captions 20

Figure Captions 20

Plasma and X-UV Source Characteristics for Al Targets Heated by 40 Nsec Nd-laser Pulses

I. Introduction

Focused power densities exceeding 10^{10} W/cm^2 are quite easily obtained with Q-switched or mode-locked laser systems. Many studies of laser-target interactions at high power densities have been performed.[1] The earliest work was done mostly with pulse lengths ≈ 10-30 nsec obtained from Q-switched devices.[2,3,4,5,6,7] Interest in thermonuclear fusion studies[8] then swung to ≈ 1 nsec CO_2 lasers and subnanosecond, mode-locked Nd:glass lasers. However, the realization of the importance of several disadvantages of very high irradiances[9] (above about 10^{15} W/cm^2 for Nd), e.g., Brillouin backscattering, low energy absorption, fast ion production, and high magnetic fields, has contributed to renewed activity at lower power densities and with multi-nanosecond pulses.

While fusion research now emphasizes plasmas with ~mm or greater extent and laser powers above the terawatt level, interest in the more modest systems continues in regard to laser-produced plasmas as x-ray sources, i.e., as converters of low-energy photons to substantially higher-energy photons.[10,11,12,13,14,15,16,17,18,19,21] The applications of the laser-plasma x-ray source include x-ray lithography[22,23,24,25] and x-ray microscopy.[26] Experimental uses include extended x-ray absorption fine structure measurement[27] and calibration sources.[28] In addition, laser-produced plasmas are uniquely suited to x-ray probing techniques during transient events such as laser-driven shock compression.[29,30] In other experiments, a knowledge of the various aspects of the energy budget of the laser-solid interaction is of interest to assess such magnitudes as the transient heating caused by x-ray absorption.[31,32,33,34] Information on the character of the x-ray and ultraviolet radiation emitted by laser-heated plasmas is needed to design applications and to properly interpret such experiments.

The present work concerns itself with x-ray source characterization, which includes determining the conditions under which the source is formed. Information on the plasma size, duration and temperature is useful for comparison with data taken with other combinations of laser pulse, focusing, and target conditions. The measurements made in this work formed the basis for the previously reported demonstration of x-ray lithography performed with this laser plasma x-ray source.[22]

X-ray emission from laser plasmas is heavily dependent on the temporal profile of irradiance. Early experiments noted a marked increase in x-ray emission when an amplified mode-locked pulse was preceded a few ns by a weak prepulse.[66,35] Aside from cratering[37] or burning through of thin film layers on specialized targets, the principal effect of a prepulse or foot on the laser pulse is one of modifying the density and temperature spatial profiles of the target, and thus influencing the laser absorption and x-ray emission processes. The elimination of prepulses has been the goal of numerous workers,[36] whereas others have sought to maximize x-ray output by varying the relative strengths of

Manuscript approved January 22, 1999.

prepulse and main pulse, typically with fixed separations not exceeding that between mode-locked pulses (about 10ns). The recent availability of short pulse (under 10ps) excimer lasers capable of generating x-ray emitting plasmas has enabled a soft x-ray (3-15 nm) emission study[38] to be made of pulse separation over the range 0-650ps. Pulse trains, each pulse effectively a prepulse for the one following by 2 ns, have demonstrated enhanced x-ray conversion.[39] Prepulse effects can be crucial in achieving x-ray lasing in laser plasmas.[40,41] The effects on x-ray yield of prepulses with μs separations have not been previously studied, and are reported here.

We have measured the x-ray emission characteristics of aluminum plasmas generated at the focus of a 2.5 GW Nd:glass laser with 40 ns pulses. This system is the same as that which was previously used for staged laser plasma-heating experiments,[42] and which we subsequently used to perform the first reported demonstration[22] of x-ray lithography with laser plasmas.[32,43,44] The lithographic results, their evaluation, and their implications have been treated in previous publications.[18,19,21] The laser plasma x-ray method was commercially developed into a submicron lithography system,[21] however successive incremental advances in UV lithographic methods reduced its competitive advantage. Laser plasma x-ray lithography continues to be considered as a contender to meet the current 0.1 μm linewidth target.

We report here on the use of a relatively long-pulse (40 ns) Nd:glass laser to irradiate planar Al targets. The laser and the target chamber are described in the next section (Section II). The laser beam focal characteristics, including temporal shape and focal conditions (total energy and average spatial distribution), were determined experimentally and are given in the third section. Then x-ray measurements with broadband PIN and sub-keV XRD (x-ray diode) detectors are introduced. The spectrally resolved x-ray results are presented in the fifth section; these include free-bound continuum slope, efficiency of converting laser light into photons above 1.5 keV, and the variations of x-ray line spectra and temperature with laser energy. Section VI presents the dependence of x-ray yield on the spacing of a prepulse from the main pulse.

II. Laser and Target Arrangement

The Nd:glass laser[42,45] used in these experiments consisted of a Q-switched oscillator and two amplifiers (Fig. 1). The output beam was 32 mm in diameter and was polarized in the horizontal plane. The laser readily produces pulses up to 100 J. There are two separate optical switches in the laser train, each consisting of a stacked plate polarizer and a quarter-wave Pockels cell (rejection ratio $\approx 10^3$:1). The first of these ((4), (5), and (6) in Fig. 1) is the Q-switch for the oscillator. The second optical switch ((11) and (12) in Fig. 1) is placed between the amplifiers (combined rod length 82cm, rod ends at Brewster's angle) and the oscillator output mirror, and helps to prevent spontaneous pre-lasing in the "external" cavity formed between this mirror and the target. A large glass turning prism directs the laser beam toward the target chamber.

The target chamber is shown schematically in Fig. 2. The laser pulses entered the diffusion-pumped vacuum system through a glass window. An f/1.9 lens, apertured as described below to an effective f/4, focused the laser pulses onto the planar targets, which were mounted on two orthogonal translation stages, one to bring the targets into focus and the second to expose fresh material for each shot. The target material was 0.125 inch thick stock aluminum 2024, an alloy containing at least 91% Al (and 3.8-4.9% Cu, 1.2-1.8% Mg, and various other constituents less than 1% each).[46] The surface was cleaned with ethanol or acetone, but not otherwise treated prior to irradiation.

Whenever a target is irradiated by a high-power laser pulse there is always the possibility of a *pre-lasing* interaction (spontaneous lasing not controlled by the Pockels cell) in the "external" cavity formed by the oscillator's sapphire output mirror and the (at least partially) reflective target. Although the external cavity of the laser is a very poor cavity, the small signal gain in the amplifiers is sufficiently high that, with even a few percent reflection returning from the target, pre-lasing can occur as much as 50 μs before the arrival of the Q-switched oscillator pulse. The amplified giant pulse, controlled by the Pockels cell, is then very small and the x-ray intensity greatly reduced. Pre-lasing is prevented by keeping the reflection from the target below about 1%. Another undesirable laser effect can arise once the Pockels cells are opened, and during the ≈150ns growth time for the oscillator. *Pulse distortions* can arise from the simultaneous oscillation of three cavities: the oscillator cavity, the external cavity, and a third cavity (having a length of ≈65 feet from retro mirror to target) formed by the combination of the two. The resultant distorted output pulse from the oscillator is a combined pulse with a slower rise and lower power. The total laser energy is very similar for a pre-lased pulse, a distorted pulse, and a Q-switched *single pulse*; however the temporal signature of each is different. A slow photodiode (50 μs/cm) which regularly monitored oscillator rod fluorescence ((8) in Fig. 1) was able to detect the long time, low level output characteristic of pre-lasing (Fig. 3b), and pulse distortions (more fully described below) were evident on a Motorola MD1 photodiode located at the target chamber. A comparison of the outputs of the photodiodes located internal to the laser, the MD1 diode at the chamber, and the resultant x-ray signals from the Al-filtered photodiode, are presented in Fig. 3.

Various approaches may be taken to reduce pre-lasing and pulse distortions. For effects which occur during the opening time of the Pockels cells, the flight time between laser and target could be increased beyond the build-up time of the oscillator. The reflectivity of the target could be defeated by a Faraday rotator, which would rotate the plane of polarization of the reflected light into a rejecting polarizer. On the other hand, surface preparations of the target are also of some help: a tilted, optically polished target returns very little light to the laser.

In this experiment, we first determined how to get clean pulses with the available target blanks. The target chamber was 15m from the turning prism at the end of the laser. Close to the chamber the beam had spread to ≈60 mm diameter and this whole diameter could be passed through a window in the target chamber and focused onto the target (Fig. 2). However, with these aluminum targets and the short focal length lens (120 mm), it was necessary to reduce the entrance aperture to 30 mm and to tilt the target ≈15° off vertical to prevent both pre-lasing and pulse distortion. This tilt directed any specularly reflected rays from the laser to an absorbing glass plate. An asymmetry in target reflectivity, due to fine factory rolling marks on the stock Al, had a minor effect on pre-lasing, depending on the orientation of the target blank. When the unwanted laser-target interactions were almost but not quite eliminated, the pulse distortion took the form of a *second pulse*. This second pulse had the same shape as the main laser output pulse but was delayed by a fixed value, i.e., the ≈100 nsec round trip time for reflections between the target and the laser. We verified that pulses were cleaner and single with tilted, optically polished aluminum blanks. (In subsequent work, we found it advantageous to sand blast and clear anodize the aluminum blanks, a treatment which is less expensive than optical polishing.)[32] While many shots had no reflected pulse, pulses below 20 joules on target were accepted if the peak height of the reflected second pulse was less than 20% of the peak height of the main pulse. Second pulse heights varied more widely on shots with >25 joules on target, but were accepted up to half the height of the main pulse, as in Fig. 3c. Pulses with more energetic reflections were not included in the data reported below, although even large reflections produced few if any x-rays, as displayed in Fig. 3d.

For the *prepulse* parameter study, we generated laser pulses with an intentional prepulse by double pulsing the Pockels cells with a first electrical pulse of 150 nsec duration, which is too short for the oscillator to build up a full power laser pulse. The duration of the resulting optical prepulse was not accurately measured, but was about the same as the main optical pulse. The main pulse is produced after a controllable delay by a 300 nsec gating pulse applied to the Pockels cells. The peak intensity ratio of the prepulse to the main pulse was about 0.2. The temporal delay τ_d between the prepulse and main pulse was varied from $\tau_d = 260$ nsec to $\tau_d = 4.5$ μs.

III. Laser Beam Characteristics

The temporal shape of the laser pulse, the total energy on target, and the energy distribution on the target at focus, are given in this section.

The overall temporal variation of the laser pulse was regularly monitored with an MD1 silicon PIN photodiode (30V bias) which was filtered to view the 1.06 μm laser light diffusely reflected from the entrance window on the vacuum chamber (see Fig. 2). The resulting electrical pulse was recorded on Tektronix 551 and 555 oscilloscopes with rise times of ≈13 nsec. This PIN detected beam temporal abnormalities, such as unwanted extra pulses and low main pulse height. Using an ITT planar photodiode and a Tektronix 519 scope (< 1 nsec rise), the laser pulse was seen to have a 40 nsec FWHM and to be somewhat asymmetric, having a 200 nsec tail which is terminated by the closure of the Pockels cell.

Throughout this experiment the Nd:glass laser was operated under constant conditions, save for the intentional introduction of a prepulse and variation of its timing for some of the shots. The main pulse energy leaving the laser was 86 J and was monitored on each shot by a carbon cone calorimeter. Of this beam energy 15% was lost at the turning prism; losses at the 30 mm diameter aperture brought the energy incident on the target chamber window down to only 51 J. Reflection losses were incurred at the window and lens. The lens used in this experiment had a 3 mm diameter hole along its optic axis and this was shadowed by a 6 mm diameter metal disc to prevent laser light reaching the ground sides of the hole. At the completion of the experiment, the total losses were 63%, so that the energy on target, for an undistorted laser pulse with no pre-lasing, was only 32 J; this value was obtained in the absence of a target by measuring the light which transited the evacuated chamber. The average reproducibility of the Nd:glass laser output energy was ±1% and the absolute calibration of the calorimetry is believed to be good to ±10%. Carbon cone calorimeters and calibrated optical attenuators were used for the calibrations. The energy on target was varied (reduced) by use of the optical attenuators.

The temporally averaged energy distribution at focus was measured using the thin film ablation technique.[47] A pair of partially reflecting flat glass plates was placed at an angle of ≈2° with respect to each other, in the beam ahead of the target chamber. A single laser shot was taken at full power but optically attenuated 100 to 300 fold. Multiple reflections between the flat glass plates produced a sequence of laterally displaced focused beams of increasing attenuation. A ≈300 Angstrom layer of Bi metal coated on a glass slide, placed at the focal plane instead of the Al target, was ablated on one shot at a series of burn spots of decreasing diameter. Microscopic measurement of the burn diameters, and knowledge of the beam energy degradation due to reflections off the plates, permitted plotting of the focal energy distribution. The result is given in Fig. 4. The irradiance (W/cm^2) for a nonattenuated focal profile is given in the same figure, using the pulse FWHM of 40 nsec and the measured total beam energy to compute the laser power. The integral of the focal

distribution is also plotted in Fig. 4, showing 30 μm to be the radius inside of which half the laser energy was incident, and $3x10^{13}$ W/cm^2 to be the irradiance reached on the beam axis. The temporally (40 nsec) and spatially (60 μm diameter) averaged irradiance on target was $1.4x10^{13}$ W/cm^2 for 86 J out of the laser (32 J on target).

The crater left in a planar target by a laser pulse is usually a rough indicator of proximity to focus, although only a weak relationship was found in work with 0.9 nsec pulses in the 1-7 Joule range.[48] In much of the early work in this field, the focal spot diameter had been identified with the crater size[14] or, more appropriately, was taken to fall between the crater size and the diffraction limit, which bounds the focal diameter within an order of magnitude in certain cases.[7] As pointed out by Stumpfel, Robitaille, and Kunze,[7] lasers can operate with multiple beamlets producing variations in divergence and pulse length across the face of the beam, leading to complications at the focus.[10]

Stereoscopic scanning electron micrographs of typical craters produced in this work are given in Fig. 5, and may be compared with the measured focal distribution in Fig. 4. At 3 J per shot, the crater diameter is ≈250 μm, and at 32 J the diameter is more than an order of magnitude larger than the half-energy diameter (60 μm) of the focal distribution. The distribution of ejected target material was measured by placing a glass plate between the lens and the target for 10 shots. The debris was found to have spattered the glass within a cone having a well defined half angle of 55 degrees.[32]

IV. Broadband X-Ray Results

The source size, history, and focal variation of x-ray intensity will be described in this section. Most data were taken for photon energies above 1 keV, although a few x-ray diode measurements were made below this energy.

A pinhole camera (Fig. 2) was employed to determine the spatial extent of the x-ray source. We used a 1.15 mm diameter pinhole in the camera obscura to record x-rays from the recombining plasma plume as well as a 25 μm diameter pinhole for higher resolution in the focal region (see Fig. 6). Measurable intensity, almost exclusively due to He-like Al ions (see below), was obtained over 1.5 cm from the target surface with the larger aperture, using Kodak Plus-X or No-Screen films. Assuming that x-ray emission occurs entirely during the laser pulse, this implies ion velocities of the order of $4x10^7$cm/s.

Two silicon PIN photodiodes, with 250 μm thick active regions and rise times of about 10-12 nsec, viewed the plasma from a distance of 89 cm, at an angle of 45° to the laser beam, as shown in Fig. 2. The detectors were rendered insensitive to visible light by fitting them with visibly opaque metal foil x-ray windows.[49] Light sealing was verified on a few shots by placing an x-ray absorbing, clear glass between the detectors and the plasma. X-ray signals were sufficiently high that relatively heavy filtration (by the foil windows) was required to avoid detector saturation on full power shots at best focus. The first detector had an aperture of 0.53 cm^2 ($\Omega = 6.7x10^{-5}$ sr) and was covered by a window[49] of 40 μm Be and 19 μm mylar, while the second had an aperture of 1 cm^2 ($\Omega = 1.26x10^{-4}$ sr) and a window of 38 μm Al. The relative detector sensitivities are given in Fig. 7a. The PIN detectors were primarily sensitive to x-rays above 2.5 and 6.5 keV, respectively, although the Be/mylar PIN will still respond (4%) to the most intense Al line. The absolute x-ray energy can be estimated using computed sensitivities for the PIN detectors.[50] The computation merely takes into account the number of photons of energy E which are absorbed in the active region of the detector, and the number of conduction electrons thereby liberated in the detector:

$$Q = \exp(-\mu_W \rho_W t)\, \exp(-\mu_{Si} \rho_{Si} d)\, [1 - \exp(-\mu_{Si} \rho_{Si} D)]\, [E_x/E_{Si}]\, q,$$

where Q is the measured charge, the μ's are the x-ray absorption coefficients (cm^2/g) and the ρ's are densities (g/cm^3), the first and second exponentials account for the x-rays lost to absorption by the window (of thickness t) and the dead layer (of thickness d) of the silicon detector, whereas the third term represents the deposition of x-ray photons in the active layer of the detector (of thickness D). For an incident x-ray photon of energy E_x, the quantity E_X/E_{Si} of signal electrons are produced, each with elementary charge q. For silicon PINs, E_{Si}=3.6 eV. The variation of PIN detected signal with laser energy, measured at best focus, is presented below (Fig. 10), where a comparison with spectrally resolved, time integrated data is made.

An x-ray pulse full width at half maximum (FWHM) of ≈10 nsec was obtained after correction of the observed FWHM (22 nsec ±10% at all laser energies used) for the response times of the detector (10-12 nsec) and the oscilloscope (≈13 nsec). (An electrical pulse, measured as 10 nsec wide on the subnsec-rise scope, gave a 22-23 nsec wide trace on the scopes used with the PINs, thus verifying the unfolding procedure.) The peak of both x-ray PIN detector signals occurred about 8 nsec prior to the laser pulse peak for 16 and 32 Joule shots, 7 nsec prior for 8 Joule shots, and 4 nsec after for 3.2 Joule shots. The absolute delay of the detector signals, which has a significant lag due to the response time of the detectors, is not to be thought of as implying that the peak of x-ray emission occurred after the peak of the laser pulse. But the increasing delay of x-ray emission with decreasing laser energy is evidence that the detected x-ray signal begins when the power density in the focal spot reaches a threshold value.

The laser irradiance was varied by enlarging the focal area by altering the lens-to-target spacing. See Fig. 7b. However, the irradiance was only measured at best focus. Hence, the intensities obtained by varying the energy on target at best focus (Fig. 10, below) cannot be directly compared with those with an enlarged focus (Fig. 7b). The decrease in x-ray intensity for enlarged foci is approximately symmetric around focus, although with a slower decrease in x-ray intensity when the target was moved toward the lens. This is consistent with the hypothesis that, for a target position in front of best focus, a substantial fraction of the plasma expands into a larger beam diameter (but lower irradiance) than at the target surface; for a target position behind (further from the laser than) best focus, an area larger than best focus is initially heated, but the part of the divergently expanding plasma which remains within the laser beam is closer to best focus and encounters a higher irradiance.

The FWHM on Fig. 7b is 0.8 mm for the effective f/4 lens. This may be compared with the anticipated depth-of-focus, defined as the axial distance over which the beam diameter remains within a chosen value. That value may be taken as the measured half-energy radius r (30 μm) of the focused laser beam. Such a value is in reasonable agreement with earlier measurements (with a 50 μm aperture) of the beam divergence half-angle alpha=3×10^{-4} rad, the focal length F=120mm, and the expression for minimum focal spot radius r=αF~35 μm. From the standpoint of geometrical optics, the focused rays are within a transverse distance r of the axis for an axial distance x on either side of the focal point, where x=2r(F/D), in which D, the initial beam diameter, is 30mm. The depth of focus is then 480 μm. It is therefore seen that there is sufficient laser energy to produce x-rays even when not at best focus.

For a few shots on a subsequent run, the PIN detectors were replaced with an Al-cathode, vacuum x-ray diode (XRD) to detect subkilovolt photons under conditions of full power and best

focus.[51] The XRD detector consisted of an approximately biplanar arrangement of photocathode and accelerating/collecting mesh held in coaxial connectors. The photocathode was a layer of at least 200 nm of aluminum evaporated on an 0.8 cm diameter, polished steel substrate;[52,53,54] the substrate, which had been soldered onto a wire prior to Al evaporation, was then inserted into the female connection of a UG-349B/U, N-to-BNC, 50 ohm coaxial adapter. The accelerating mesh, made of 200 lines/inch electroformed Ni with 78% open area, was spaced away from the photocathode by a metal cylinder which contacted the casing of the coax adapter. Enclosing the diode was a metal housing made of the casing of a mating UG-59B/U cable connector. The x-ray flux entered the diode through the opening in this casing, passed through the mesh, and impinged on the photocathode. An aperture and various x-ray filters were conveniently held in the casing. The aperture prevented direct illumination from the plasma from reaching internal surfaces other than the mesh and cathode.

Since biplanarity was not precise and the ascertainment of cathode-mesh spacing was difficult in this design (thought to be 0.5-1.5 mm), the normal bias of -300V was extended to -500V on one shot. It was verified that the signal level did not increase at the higher voltage, to within the rather sizeable shot-to-shot variation (see below). An increase would have implied a raising of the space-charge limited current capacity of the diode due to the increased bias. Space charge limited flow, for which the detector is in saturation, occurs in a parallel biplanar geometry when the current density of emitted (low velocity) electrons j reaches the value:

$$j = (4/9)(2\ e/m)^{1/2}\epsilon_o\ |V|^{3/2} / d^2,$$

where $\epsilon_o = 8.85 \times 10^{-12}$ farad/meter and $e/m = 1.7589 \times 10^{11}$ coulomb/kg.
Amalgamating constants, this becomes

$$j = 2.34 \times 10^{-6}\ |V|^{3/2} / d^2, \qquad \text{Eqn. (1)}$$

where V is the potential in Volts, and d is the spacing between the biplanar electrodes in cm, for j in amperes/cm^2.[55,57] Deviations from this limiting value have been reported in XRDs, where either the mesh transmission was low (0.64) or insufficient charge was made available to the detector during the pulse.[57] Evidently, this increase is primarily a matter of how one defines the areas of interest, and is not a local violation of Eqn. (1). One would expect the current not to exceed that attained without a mesh, a consideration which is least significant for the more highly transmissive meshes. Taking all this into account, a 10 V signal recorded through 50 Ω line would be expected to saturate our detector if the diode spacing were increased to somewhat over 2 mm; this calculation agrees with our observation that the diode was not saturating.

The voltage traces of the XRD were recorded on shots ranging from 30-36 J on target, at best focus. The traces had a width equal to that of the laser pulse, i.e., wider than the kilovolt x-ray emission; the lower photon energies sensed by the XRD are present for a longer time than the peak temperatures needed to produce the more energetic x-ray photons. Occasionally the laser would produce a weak trailing pulse, which was sufficient to excite plasma radiation detectable by the XRD. A glass sheet placed in front of the XRD removed all detected signal, as expected. (This detector is not sensitive to visible light, since single-photon absorption provides insufficient energy for an electron to be emitted.) The XRD was operated without filtration (bare), and was also operated with a thin foil photon filter over the aperture. The filtered XRD gave about 20x less signal than the bare, for both 0.5 μm Al and for 2 μm Kimfoil[56] filters.

The XRD signals were integrated to give coulombs/sr detected signal, taking into account the 3.3×10^{-5} sr solid angle of the apertured photocathode. The values are given in Table I. Neither the filters nor the XRD were calibrated, nor was the subkilovolt spectrum measured. Nonetheless, a rough estimate can be made of the plasma's subkilovolt photon emission, based on the measurements in Table I and published sensitivities for similar XRDs with aluminum cathodes.[52,53] In the <0.1 keV photon energy range, the quantum efficiency (number of signal electrons generated per photon incident) of the aluminum (oxide) photocathode displays a broad peak at about 14 eV with a value approaching 0.2;[54] however, these low energy photons do not contribute greatly to the total energy in the photon spectrum, since they occupy only a small spectral range as compared to 0.1-1.0 kilovolt and higher energy photons. The total quantum yield for an Al film photocathode in the 0.1-1.0 keV range[52] has a minimum value of about 6×10^{-2} just below the 0.52 keV oxygen K edge, a maximum ten-fold greater on the high energy side of the edge, and a broad maximum of 5 or 6×10^{-1} below about 200 eV photon energy. The sensitivity above the aluminum K-edge (1.49 keV) is nearly identical to that at the oxygen edge;[52] the detector therefore has a significant response to the above-kilovolt features of the plasma radiation spectrum. Taking a nominal value of 3×10^{-4} coulombs/sr and 30 Joules for the unfiltered diode, gives 10^{-5} c/(J-sr) conversion efficiency into detected signal. After converting this to signal electrons/(J-sr) and applying the extreme values for quantum efficiency in the range 0.1-5.0 keV, the conversion efficiency from laser light to detectable emitted photons is seen to fall within about 3×10^{12} and 3×10^{13} photons/(J-sr). Removing the number of above-keV photons present in the spectrum (deduced from results presented below) merely lowers the range of sub-kev photons to 2×10^{12} - 3×10^{13} photons/J-sr. If these photons were monoenergetic at 100 eV, the energy conversion of laser light into detected sub-keV photons would be no greater than a fraction of a percent. Other workers, also viewing at only one angle but operating with larger focal spots at 3×10^{4} W/cm^2 on Al discs and 0.97ns pulse lengths, found two percent conversion into 2π sr, with a decrease in conversion at yet higher irradiances.[58]

Table I, XRD Signals

Filter	Joules	Volts	coulombs/sr
bare	30	-300	2.3×10^{-4}
"	30	"	2.4 "
"	32	"	3.2 "
"	34	-500	3.3 "
2 μm Kimfoil	34	-300	1.2×10^{-5}
"	36	"	1.4 "
0.5 μm Al	34	"	1.1 "
"	33	"	1.2 "
glass + Al	34	"	$<6.3 \times 10^{-7}$

V. X-Ray Spectral Studies

X-ray spectra were measured as a function of incident energy, were spectrally integrated to obtain total x-ray intensity, and were used to estimate electron temperatures. Broadband x-ray

intensities, obtained as a function of irradiance with the PIN detectors by varying the laser energy, are presented in this section alongside comparable spectrally resolved data. (For x-ray output as a function of laser focal position, see Fig. 7b, above).

X-ray spectra were recorded with the single-crystal spectrograph sketched in Fig. 2. The crystal was a 6.3 cm long, flat piece of KAP (potassium acid phthalate); the x-ray film was positioned in an opaque holder behind a 25 μm Be filter.[49] Kodak No-Screen Medical X-Ray Film was used throughout in this experiment for quantitative intensity measurement, since this was the first x-ray film for which a comprehensive model was available with which to calculate photometer and film response in the soft x-ray region.[59] (No-Screen and its developer are no longer available; the replacement film is Direct Exposure Film DEF.) The center of the crystal was located at a horizontal angle of 45° to the laser axis. Strips of mylar foil (0., 12, 25, 31 μm) over the Be served as x-ray attenuators to provide a wide dynamic range on a single shot. The x-ray spectra were scanned with a Grant microdensitometer (28X lens, acceptance angle 23°, numerical aperture 0.39) and digitally recorded. The photometer operated at a dark current density which ranged between 5.0 and 5.5 optical densities (OD), where the density of an unexposed, fixed, blank sample of film was 0.06 OD, and a typical value for a new, unexposed, properly developed[60] blank was 0.32 OD above the fixed blank. Data films had fog levels within 0.03 OD of the developed blank, indicating that the films were new when used. The darkest line in the data set attained 3.62 OD above fixed blank, in a region of the spectrum unfiltered by mylar foil; that is, dark current levels had essentially no influence on density readings. A computer program[61] converted the scan records to tabular output and plots by correcting for the computed crystal reflectivities,[62] film efficiency,[59,60] filter absorption coefficients,[63] and spectrograph geometry (including crystal dispersion).[64]

After all the above corrections had been applied, six points from the data set at 1.60 keV were examined for consistency with the H&D curve. In this check, the high density exposure on a given film was assumed to have been correctly computed. A lower density reading ($1.0 < OD < 2.0$) from the same film was directly converted to exposure from the H&D curve; this was then compared with the exposure expected from the high density point. The expected exposure was calculated by correcting the high density exposure for the attenuation by the mylar layer(s) placed in front of the low density portion of the film during the experiment. The assumed thickness of the mylar was then adjusted to improve the comparison. The closest agreement was obtained by thinning the manufacturer's thickness figures for the mylar by a factor of $f=0.91$. The adjusted data scattered about the H&D curve within the ranges $f \approx 0.88$ to 0.96 near $OD \approx 1$, and $f \approx 0.8$ to 1.08 at $OD \approx 1.8$. The reason for the scatter is not known, but may be due to (1) actual variations in mylar thickness (which would introduce scatter into the final reported data points[49]), (2) an unreliability of development procedures at high density[65] (which would not affect the reported data, as they do not include the high density points), or (3) the fact that the H&D curve above $OD \approx 2.8$ is strongly dependent on a single nearby experimental calibration point at 1.49 keV[60] (again, not a matter of concern for the reported data). Exposure values reported in this paper were computed from the unmodified, nominal mylar thicknesses given by the film manufacturer.

The redrawn computer-generated spectral plots are presented in Fig. 8, while the tabular computed output, which was used to calculate the integrated intensities (above background) of x-ray lines, is presented in Table II. The resonance line of the helium-like Al ion was resolved from and (for the higher powered shots) much more intense than the neighboring intercombination line and dielectronic satellites.[66] Manual deconvolution on the plotted spectra, followed by planimetry, sufficed to obtain resonance line integrals; these integrals agreed with those obtained from the tabular

output. A free-to-bound continuum spectrum, corrected as were the line spectra but plotted with semilog coordinates, is given in Fig. 9. Further discussion of the details of the line and continuum spectra is given below.

A low-energy spectral measurement, using a McPherson model 235 Seya-Namioka spectrograph, was also made. The spectrometer viewed the plasma at a small angle to the target surface. A weak spectrum in the 10 to 40 eV range was obtained in 4 shots, at 32 J per shot, using a 1200 L/mm grating and Kodak 101-04 film. Line identifications showed that the low energy spectrum consisted primarily of lines from Al X and Al XI. The low energy spectrum is dominated by radiation from lower ionization stages in contrast to the x-ray spectrum which arises from higher ionization stages. We were not able to follow the stages of ionization down with decreasing laser irradiance, owing to loss of signal strength. Improvements in signal strength could be made by redesigning the target chamber or spectrograph to permit closer coupling from plasma to detector.

Absolute x-ray intensities obtained for individual lines, after applying the above-mentioned corrections, are given in Table II for energies on target ranging from 3 to 32 J. The laser energy was varied in this range by optical attenuators, keeping the focal conditions fixed. In some cases, multiple shots (each a fresh area of Al target) were recorded in one spectrum by the KAP spectrograph to increase the photographic density. The variation of relative line intensities with laser energy is particularly evident in Fig. 8 for the group of lines near 1.6 keV.

Table II

J/shot	W/cm^{-2}	C.F. ev/sr	Tot XR ev/sr	He-res ev/sr	H-res	He/H	Shot(s)
32.0	2.80E+13	4.92E-03	7.83E+16	2.68E+16	8.22E+14	3.07E-02	1522
32.0	2.80E+13	3.01E-03	4.79E+16	3.07E+16	1.04E+15	3.39E-02	1571
32.0	2.80E+13	3.00E-03	4.77E+16	3.06E+16	6.48E+14	2.12E-02	1524
26.0	2.28E+13	1.69E-03	2.19E+16	1.36E+16	3.06E+14	2.25E-02	1528
21.0	1.84E+13	1.50E-03	1.57E+16	9.85E+15	1.44E+14	1.46E-02	1531
16.1	1.41E+13	1.06E-03	8.48E+15	5.24E+15	3.60E+13	6.87E-03	1561-70
16.0	1.40E+13	7.79E-04	6.20E+15	3.27E+15	1.05E+13	3.21E-03	1525
13.0	1.14E+13	5.37E-04	3.47E+15	1.89E+15			1532
7.5	6.52E+12	1.60E-04	5.93E+14	2.80E+14			1542-46
8.0	7.00E+12	1.22E-04	4.86E+14	2.44E+14			1526
3.2	2.77E+12	1.42E-05	2.23E+13	7.13E+12			1547-56

Table II. X-ray spectrographic data, on a per-shot basis. J/shot and W/cm^2 column give laser quantities on target. C.F. gives conversion fraction of total x-rays into 4πsr (calculated as though isotropic) normalized to laser energy on target. Helium resonance line intensities were unfolded from neighboring satellites and intercombination line. For lower irradiance shots, the hydrogenic line intensities were too weak to measure reliably.

Integrated absolute x-ray intensities, obtained from spectrally integrating the crystal spectrograph data and temporally integrating the PIN signals are given in Table II, and also plotted in Fig. 10. The maximum intensity of emitted x-rays observed by the spectrograph was 1.25×10^2 J/sr, which corresponds to a conversion of 0.25%, if the x-ray energy is assumed to be isotropically radiated into 2π steradians. The spectrograph and the Be-mylar filtered PIN indicate that the intensity of emitted x-rays increases with the 3.2 power of the laser energy (or the irradiance). The apparent discrepancy between the absolute magnitudes plotted for the spectrograph and PIN is caused by the photon energy regions sampled by the different detectors. The spectrograph recorded K lines and free-to-bound continuum; for 30 Joule shots, 85±5% of the measured photon energy was in lines at 1.6±.04 keV (Table II), where the PIN is not very sensitive (see Fig. 7a). Hence, the PIN-recorded intensities are substantially smaller than those obtained with the spectrograph.

The power dependence of the broadband x-ray emission has been measured by other workers operating with different lasers and under different conditions, yet obtaining very similar results to those reported here. An exponent of 3 was found in an experiment with 1.06 μm, 3 nsec pulses at irradiances above ours up to 2×10^{14} W/cm^2 on Al slabs.[67] An experiment with a CO_2 laser, with 60 nsec pulses focused to 3×10^{10} to 1.2×10^{12} W/cm^2 on Al and other targets, also determined the broadband x-ray emission to vary approximately as the third power of the irradiance.[68]

A quantitative comparison can be made between the PIN and the spectrograph. The corrected line spectrum can be computationally attenuated by Be and mylar according to the PIN filtration and compared with the observed PIN signal. This was done, attenuating three energy cuts of the line spectrum, for a laser energy of 13 Joules at which the PIN output would be 1.0 volt. The transmitted line energy was then converted to a voltage (3.6 eV per electron-hole pair), and was plotted as a box in Fig. 10; the agreement with the Be/mylar PIN is quite good, implying that there is little continuum above the spectrograph's upper limit of about 3 keV. Even after filtration by beryllium and mylar, the majority of the detected PIN signal is from the lines at 1.6 keV.

Plasma electron temperature determinations from x-ray spectra are strongly influenced by the degree of spatial and temporal integration inherent in making an actual measurement. Self-absorption (opacity), gradients,[69] transient effects in atomic level populations,[70] and the possible existence of non-Maxwellian electron distributions[71,72] can all complicate the interpretation of the spectrum. The degree to which any inferred temperatures properly represent actual conditions in the plasma is dependent on the validity of the plasma emission model employed for comparison with the spectral features of the experiment, whether they be lines or continuum. Under such conditions, measurements may yield more of an apparent plasma temperature than a true value. Significant improvements in experimental method, involving the techniques of tracer spectroscopy to remove spatial averaging, have been introduced by Whitlock[73] and Herbst and coworkers,[74] and by Ripin and Whitlock.[75] Although the present experiment does not make use of the tracer techniques, we shall examine the results as a basis for at least a semiquantitative comparison to other similar work.

Ratios of the line intensities in Table II may be used to estimate electron temperatures according to any of several models. Interpreting these line ratios with a coronal model[76] shows a decrease of about 100 eV in inferred temperature for a factor of two drop in laser energy (see Fig. 11). It is interesting to compare this result with a temperature obtained from the slope of the free-to-bound continuum. The recombination continuum shown in Fig. 9 was sufficiently intense to yield a useful slope only for 32 J shots; an electron temperature of 230±40 eV is consistent with the observed slope. This value is significantly below those from lines via the coronal model, but is considered to be the

better estimate of the actual plasma temperature, owing to the broad bandwidth, relative simplicity of the thermalization process and the shorter thermalization times of free electrons compared to bound electrons.[77,78]

The influence of laser irradiance on apparent plasma temperature has received a great deal of attention worldwide for many years. An indication of the range of results reported in some two dozen experiments is presented in Fig. 5 of Gitomer, et alii,[79] where a logarithmic plot, of the form first presented by Giovanielli,[80] gives T_e plotted against 9 orders of magnitude of the product of intensity I times the square of the laser wavelength λ. The temperature of interest in their paper is the maximum or hot electron temperature, which merges with the so-called cold electron temperature at the irradiances of interest in the present work. While, in their figure, the electron temperature T_e at any irradiance spans almost an order of magnitude, they find an approximate overall trend to be described by $T_e \approx a(I\lambda^2)^b$, where T_e is in eV, a is a constant, $I\lambda^2$ is in units of (W cm^{-2} μm^2), and the exponent b has the value 4/9. In the region of $I\lambda^2 \approx 10^{13}$ W/cm^2, the figure of Gitomer, et al., is somewhat underfilled with data; the values we report would fall between the swaths of points on their plot at higher and lower irradiances.

VI. Effect of Prepulse on X-Ray Output

As detailed in Section II, a prepulse with controllable separation from the main pulse could be reliably produced with this laser. Hence an exploratory study of prepulse effects on long-pulse interactions was made. The prepulse was roughly 20% of the main pulse, and preceded the main pulse by >0.2 μs, shown in the inset to Fig. 12. The integrated x-ray intensity recorded using the PINs was found to be smaller with a prepulse than without. The results are given in Fig. 12. A minimum in the x-ray output occurred at a prepulse spacing of $\tau_d = 0.5$ μs. Larger and smaller separations produced greater output than the minimum. A prepulse more than 4 μs ahead of the main pulse yielded only 60-70% as much x-ray intensity as a shot with no prepulse, for both PINs. The delay τ_d has an upper limit associated with the lifetime of the prepulse-induced plasma, because the absence of plasma allows the main pulse to see the prepulse's reflective crater, which would induce a laser-target interaction in the external cavity and spoil the main pulse. This upper limit was not reached in the data of Fig. 12 (due to the limits of the laser), but was verified experimentally by taking two successive shots ($\tau_d = 5$ min, first pulse was 10% of the second) onto the same area of target.

Conclusions

The total laser energy temporal history and focal energy distribution for 40 nsec, 1.06 μm Nd:glass laser interactions with planar Al targets were measured. Laser-produced plasma emissions within the 10 eV - 3 keV ultraviolet and x-ray range were recorded. The dependence of kilovolt x-ray emission on laser irradiance was obtained by altering the energy on target and the lens-target spacing. Emitted x-ray intensity over this range of photon energy was found to increase as the 3.2 power of laser energy at best focus. A maximum efficiency attained (under these conditions) for conversion of incident laser energy to radiation above 1.5 keV was 0.25% into 2π sr. Temperatures obtained from x-ray line intensity ratios showed a decrease at lower irradiances. Values near 230 eV were obtained from free-bound continuum shape for 3×10^{13} W/cm^2 peak irradiance. Prepulses arriving up to 4 μs ahead of the main pulse reduced the overall x-ray output, with the greatest reduction at 0.5 μs pulse separation. While previous studies do not duplicate the conditions and measurements employed here, our x-ray results are consistent with related experiments performed at other laboratories.

Acknowledgements

We wish to acknowledge the dedicated technical assistance of the late James Cheadle, whose persistence despite illness remains an inspiration. We also appreciate the use of the multipass mirrors provided by B.H. Ripin, and the support provided by R.E. Pechacek throughout the experiment.

References

1. T.P. Hughes, Plasmas and Laser Light, (J. Wiley, N.Y., 1975).

2. "A spectroscopic study of the plasma generated by a laser from polyethylene,"
B.C. Boland, F.E. Irons, and R.W.P. McWhirter, J. Phys. B(Proc. Phys. Soc.), Ser. 2, Vol. 1, 1180-91 (1968).

3. "Measurement of the time variation of the temperature of the plasma of a flare by means of its x-radiation,"
N.B. Basov, V.A. Boiko, B.A. Gribkov, S.M. Zakharov, O.N. Krokhin, and G.V. Sklizkov, JETP Ltrs. 9, 315-17 (1969).

4. "Temperature in laser-created deuterium plasmas,"
J.L. Bobin, F. Delobeau, B. De Giovanni, C. Fauquignon, F. Floux, Nuclear Fusion 9, 115-20 (1969).

5. "Temperature and expansion energy of laser produced plasmas, II. Experiments,"
H. Puell, H.J. Neusser, and W. Kaiser, Z. Naturforsch. 25a, 1815-22 (1970).

6. "Temperature measurements of a laser-produced plasma using the recombination continuum,"
W. Seka, C. Breton, J.-L. Schwob, and C. Minier, Plasma Physics 12 73-77 (1970).

7. "Investigation of the early phases of plasma production by laser irradiation of plane solid targets,"
C.R. Stumpfel, J.L. Robitaille, and H.-J. Kunze, J. Appl. Phys. 44/3, 902-7 (1972).

8. J. Knuckolls, L. Wood, A. Thiessen, and G. Zimmerman, Nature **239**/5368, 139-42 (1972).

9. B.H. Ripin, R.R. Whitlock, F.C. Young, S.P. Obenschain, E.A. McLean, and R. Decoste, "Long-Pulse Laser-Plasma Interactions at 10^{12}-10^{15} W/cm^2," Phys. Lett. 43, 350 (1979).

10. "X-ray emission from laser-produced magnesium plasmas,"
T.N. Lee and D.J. Nagel, J. Appl. Phys. 46/9, 3784-88 (1975).

11. "Spectroscopic study of laser created aluminum plasma,"
J.C. Couturaud, Opt. Comm. 22/1, 71-4 (1977).

12. "Plasma x-ray emission produced by ruby lasers at 10^{12} W/cm^2,"
R.D. Bleach and D.J. Nagel, J. Appl. Phys. 49/7, 3832-40 (1978).

13. "X-Ray Yields of Plasmas Heated by 8-Nsec Neodymium Laser Pulses,"
K.M. Glibert, J.P. Anthes, M.A. Gusinow, M.A. Palmer, R.R. Whitlock and D.J. Nagel, J. Appl. Phys. 51/3, March 1980, pp. 1449-1451.

14. "Study of x-ray emissions from a copper plasma produced by a laser,"
B.K. Sinha and N. Gopi, Phys. Fluids 23/8, 1704-9 (1980).

15. "Repetitively-pulsed-plasma soft x-ray source,"
D.J. Nagel, C.M. Brown, M.C. Peckerar, M.L. Ginter, J.A. Robinson, T.J. McIlrath and P.K. Carroll. Applied Optics, 23/9, (May, 1984), 1428-33.

16."Soft x-ray lithography using radiation from laser-produced plasmas,"
P. Gohil, H. Kapoor, D. Ma, M.C. Peckerar, T.J. McIlrath and M.L. Ginter, Appl. Opt.24 (July, 1985), 2024-7.

17. "X-ray lithography using a KrF laser-plasma source,"
F. O'Niell, M.C. Gower, I.C.E. Turcu, and Y. Owadano, Appl. Opt.25/4, 464-5 (1986).

18. "X-Ray Lithography Research: A Collection of NRL Contributions,"
R.R. Whitlock, NRL-MR 5731 (24 Aug., 1987).

19. "Incoherent x-rays from laser-heated plasmas,"
D.J. Nagel, in **High Intensity Laser Processes**, SPIE Vol. 664, Society of Photo-Optical Instrumentation Engineers, Bellingham, WA, 142-150 (1986).

20. "Plasma Sources for X-ray Lithography,"
D.J. Nagel, in **VLSI Electronics: Microstructure Science, Vol. 8.**, N.G. Einspruch, ed., Academic Press, Ch. 6 (1984).

21. Hampshire Instruments, formerly of Marlborough, MA.

22. D.J. Nagel, R. R. Whitlock, J. R. Greig, R. E. Pechacek, and M.C. Peckerar, presented to SPIE conference on Developments in Microlithography, 9-11 April 1978, San Jose, CA.

23. "Conversion efficiency of laser radiation into soft x-ray radiation of laser produced plasmas for x-ray lithography,"
M. Kuehne and H.-C. Petzold, Microelectron. Eng. (Netherlands)3/1-4, 565-71 (1985).

24. "X-ray sources for microlithography created by laser radiation at l=0.26mm,"
H. Pepin, P. Alaterre, M. Chaker, R. Fabbro, B. Faral, I. Toubhans, D.J. Nagel, and M. Peckerar, J. Vac. Sci. Technol. B 5/1, p.27-32 (1987).

25. "Laser plasma x-ray sources for microlithography,"
M. Chaker, H, Pepin, V. Bareau, B. Lafontaine, I. Toubhans, R. Fabbro, and B. Faral, J. Appl. Phys. 63/3, 892-9, 1988.

26. "Laser produced plasma VUV and soft x-ray light sources,"
M.L. Ginter, in X-Ray Microscopy, Proc. Int'l. Symp, Springer Verlag, New York, 25-29 (1984);
"Soft x-ray contact microscopy with nanosecond exposure times,"
R.J. Rosser, K.G. Baldwin, R. Feder, D. Bassett, A. Cole, and R.W. Eason, J. Microscopy, Vol 138, Pt.3, 311-319 (June, 1985).

27. R.W. Eason, D.K. Bradley, J.D. Kilkenny, and G.N. Greaves, J. Phys. C, 17, 5067 (1981);
P.J. Mallozzi, R.E. Schwerzel, H.M. Epstein, and B.E. Campbell, Phys. Rev. A, 23, p. 824 (1981);
"Reflection extended x-ray absorption fine structure recorded using a laser-produced plasma x-ray source,"
R.W. Eason, D.K. Bradley, P.J. Dobson, and J.D. Hares, Appl. Phys. Lett. 47(5), 442-4 (1985);
"Improved laser-EXAFS studies of aluminum foil,"
R.W. Eason, D.K. Bradley, J.D. Kilkenny, and G.N. Greaves, J. Phys. C: Solid State Phys., 17 p.5067-74 (1984).

28. "Negative Resist dose characteristics measurements by laser plasma soft x-ray source," V.P. Avtonomov, Yu.G. Geonjian, A.V. Orlov, G.V. Sklizkov, L.K. Subbotin, and A.M. Checkmarev, Microelectron. Eng. (Netherlands) **3**/1-4, 623-9 (1985).

29. "The Study of Shock Launching in Silicon by Pulsed X-Ray Diffraction," J.S. Wark, R.R. Whitlock, A. Hauer, J.E. Swain and P.J. Solone, Rapid Communications, Phys. Rev. B **35**/17, 15 June 1987, 9391-4.

30. "Orthogonal Strains and Onset of Plasticity in Shocked LiF Crystals," R.R. Whitlock and J.S. Wark, Physical Review B, **52**/1, 1 July 1995, 8-11.

31. "Laser Processing of High-Tech Materials at High Irradiance," Robert R. Whitlock, NRL Memorandum Report 5915, 3 February 1987.

32. "High Speed X-Ray Lithography with Radiation from Laser-Produced Plasmas," M.C. Peckerar, J.R. Greig, D.J. Nagel, R.E. Pechacek and R.R. Whitlock, Proceedings of the 8th International Symposium on Electron and Ion Beam Science and Technology, R. Bakish, ed., Vol. 78-5, The Electrochemical Society, Inc., Princeton, NJ (May, 1978), 432-441.

33. "Preheat studies for foils accelerated by ablation due to laser irradiation," E.A. McLean, S.H. Gold, J.A. Stamper, R.R. Whitlock, H.R. Griem, S.P. Obenschain, B.H. Ripin, S.E. Bodner, M.J. Herbst, S.J. Gitomer, and M.K. Matzen, Physical Review Letters 45/15, 13 October 1980, pp. 1246-1249; and NRL Memorandum Report 4356, October 13, 1980.

34. "The effect of high x-ray fluxes on laser-plasma x-ray spectrometers," J.S. Wark and R.R. Whitlock, Rev. Sci. Instrum. **64**/7, July 1993, 1718-1722.

35. D.J. Nagel, P.B. Burkhalter, G.A. Doschek, C.M. Dozier, U. Feldman, B.M. Klein, and R.R. Whitlock, in NRL Report 7838, "Laser Fusion Studies at NRL - A Report to the AEC for the Period July 1973 to June 1974," J.A. Stamper and L.S. Levine, eds., p. 98 (1974) (unpublished).

36. D. Riley, L.A. Gizzi, F.Y. Khattak, A.J. Mackinnon, S.M. Viana, and O. Willi, Phys. Rev. Lett. **69**, 3739 (1992).

37. J.A. Cobble, G.T. Schappert, L.A. Jones, A.J. Taylor, G.A. Kyrala, and R.D. Fulton, J. Appl. Phys. **69**, 3369 (1991).

38. U. Teubner, G. Kuehnle, and F.P. Schaefer, Appl. Phys. B **54** 493-9 (1992).

39. F. O'Neill, I.C.E. Turcu, D. Xenakis, and M.H.R. Hutchinson, Appl. Phys. Lett. **55** 2603 (1989).

40. J.Nilsen, B.J. MacGowan, L.B. Da Silva, and J.C. Moreno, Phys. Rev. A **48**/6, 4682 (1993).

41. "Thin foil x-ray converters pumped by subpicosecond excimer lasers," D.E. Casperson, J.A. Cobble, R.D. Fulton, G.A. Kyrala, G.T. Schappert, A.J. Taylor, and E. Wahlin, Journal of Applied Physics, **74**/6, 3707-11 (1993).

42. J.R. Greig and R.E. Pechacek, J. Appl. Phys. 48, 596-604 (1977); and J.R. Greig, J. Appl. Phys. 48, 5382 (1977).

43. "Lithography and High-Resolution Radiography with Pulsed X-Rays,"
D.J. Nagel, J.M. McMahon, R.R. Whitlock, J.R. Greig, R.E. Pechacek, and M.C. Peckerar, Proceedings of the International Conference on X-Ray and XUV Spectroscopy, Sendai, Japan, published in the Japanese Journal of Applied Physics, 17, (1978) Supplement 17-2, pp. 472-475.

44. "Submicrosecond X-ray Lithography,"
D.J. Nagel, M.C. Peckerar, R.R. Whitlock, J.R. Greig and R.E. Pechacek, Electronics Letters 14/24, 23 Nov. 1978, pp. 781-2.

45. J.R. Greig and R.E. Pechacek, NRL-MR 3461 (1977) unpublished.

46. Federal specification QQ-A-250/4E, per Mr. Bolt, Naval Research Laboratory, private communication.

47. B.H. Ripin, in NRL-MR 3315 (1976), S.E. Bodner, ed., p. 20-22, 44-45, unpublished.

48. "Craters produced by high power-density lasers,"
R.D. Bleach and D.J. Nagel, manuscript 75-WA/HT-49, Amer. Soc. of Mech. Eng., (1975).

49. "Thickness Variations in X-Ray Filters and Laser Targets,"
R.R. Whitlock and J.A. Sprague, Applied Physics Letters 45/5, 1 Sept. 1984, pp. 504-6.

50. "Sensitivity of Solid State Detectors to Fluorescent X-Rays,"
P.J. Ebert and H.N. Kornblum, Lawrence Radiation Laboratory report UCID-15278, (Sept. 7, 1967), unpublished, and J.J. Hohlfelder, "Measurement of the Sensitivity of Silicon Diodes in the Energy Region 1.8 to 5.0 keV," in Advances in X-Ray Analysis Vol. 17 (Plenum, 1974), p. 531-541.

51. "New detector for the vacuum ultraviolet,"
R. Lincke and T.D. Wilkerson, Rev. Sci. Instrum. 33(9), 911-913 (1962).

52. "The characterization of x-ray photocathodes in the 0.1-10 keV photon energy region",
B.L. Henke, J.P. Knauer, and K. Premaratne, J. Appl. Phys. 52(3), 1509-20 (Mar. 1981).

53. "Photoelectric quantum efficiencies and filter window absorption coefficients from 20 eV to 10 keV,"
R.H. Day, P. Lee, E.B. Saloman, and D.J. Nagel, J. Appl. Phys. **52**/11, 6965-73 (1981); and LA-MS-7941, Mar. 1981.

54. "Metal photocathodes as secondary standards for absolute intensity measurements in the vacuum ultraviolet,"
R.B. Cairns and J.A.R. Samson, J. Opt. Soc. Am. 56(11), 1568-73 (1966).

55. P.T. Kirstein, G.S. Kino, W.E. Waters, Space-Charge Flow, McGraw-Hill, NY 1967, p. 51.

56. Kimfoil C16 H14 O3, per B.L. Henke and E.S. Ebisu, *Adv. X-Ray Anal.* vol. 17, C.L. Grant, C.S. Barrett, J.B. Newkirk, and C.O. Ruud, eds., Plenum Press, NY (1974) pp. 150-213, p. 211.

57. "A study of bare x-ray diode saturation due to a high fluence x-ray pulse,"
R.B. Spielman and J.P. Anthes, Proc. Topical Conf. on Low Energy X-Ray Diagnostics, AIP Conf.

Proc. No. 75, 278-9 (1981);

58. "Time Resolved, Sub-keV X-Ray Measurements Using Filtered X-Ray Diodes," K.G. Tirsell, H.N. Kornblum, and V.N. Slivinsky, UCRL-preprint 81478, 18 Aug. 1979.

59. "The sensitivity of x-ray films: Part I, a model for sensitivity in the 1-100 keV region," D.B. Brown, J.W. Criss, and L.S. Birks, J. Appl. Phys. **47**, 3722-31 (1976).

60. "The Sensitivity of X-Ray Film: Part II, Kodak No-Screen Film in the 1 to 100 keV Region," C.M. Dozier, D.B. Brown, L.S. Birks, P.B. Lyons, and R.F. Benjamin, JAP 47, p. 3732-39 (1976).

61. XTALFILM. R.R. Whitlock and J.W. Criss, unpublished.

62. "Integral Reflection Coefficient of X-Ray Spectrometer Crystals," J.V. Gilfrich, D.B. Brown, and P.G. Burkhalter, Applied Spectroscopy 29, 322 (1975).

63. W.J. Viegele, E. Briggs, B. Bracewell and M. Donaldson, X-Ray Cross Section Compilation, (Kaman Nuclear Corp., revised 1971, DNA 2433F Vol. 1 Rev. 1, KN-71-431(R)).

64. J.W. Criss, Applied Spectroscopy **33**, 19 (1979), and errata (to Eqs. 14, 20, A-4, and to Sect. IVA) **33**, 426 (1979).

65. C.E. Mees and T.H. James, The Theory of the Photographic Process, 3rd Edition, (Macmillan Co., New York, 1966).

66. "Satellite Spectra from Laser-Produced Plasmas," U. Feldman, G.A. Doschek, D.J. Nagel, R.D. Cowan and R.R. Whitlock, Astrophysical Journal 192, pp. 213-220, Aug. 15, 1974.

67. "X-ray emission from aluminum laser produced plasma," J.C. Coutraud, C. Faure, and J.L. Rocchiccioli, in Proc. Twelfth Int'l. Conf. on Phenomena in Ionized Gases, Part 1, J.G.A. Hoelscher and D.C. Schram, eds., American Elsevier Pub. Co., Inc., NY (1975).

68. "The interaction of CO_2 laser radiation with various solid targets," P.E. Dyer, S.A. Ramsden, J.A. Sayers, and M.A. Skipper, J. Phys. D: Appl. Phys. 9, 373-82 (1976).

69. "Spectroscopic diagnostics of laser plasmas," Ch. 13 in George Bekefi, Claude Deutsch, and Barukh Yaakobi, in Principles of Laser Plasmas, G. Bekefi, ed., John Wiley & Sons, New York, p. 587 (1976).

70. "Soft x-ray spectroscopic diagnostics of laboratory plasmas," C. De Michelis and M. Mattioli, Nuclear Fusion **21**/6, 677-754 (1981).

71. "Validity of electron-temperature measurements using continuum plasma emission," M. Lamoureux, C. Moeller, and P. Jaegle, J. Quant. Spectrosc. Radiat. Transfer**33**/2, 127-131 (1985).

72. M.H. Key, J. Phys. B 8, 674-83 (1975).

73. "X-Ray Studies of Tracers in Laser-Produced Plasmas,"

R.R. Whitlock, B.H. Ripin, M.J. Herbst, P.G. Burkhalter, and J. Grun, Fourth APS Topical Conference on High Temperature Plasma Diagnostics, Boston, MA, August 25-27, 1982, Bulletin of the American Physical Society 27/7, Sept. 1982, p. 825.

74. "New Measurement Techniques Using Tracers within Laser-Produced Plasmas," M.J. Herbst, P.G. Burkhalter, D. Duston, M. Emery, J. Gardner, J. Grun, S.P. Obenschain, B.H. Ripin, R.R. Whitlock, J. Apruseze and J. Davis, Sixth International Workshop on Laser Interactions Related Plasma Phenomena, Monterey, CA, 25-29 Oct. 1982.

75. "Radiative Opacity and Emissivity Measuring Device," B.H. Ripin and R.R. Whitlock, U.S. Patent No. 4,597,933, dated 1 July 1986.

76. "Coronal equilibrium of high-atomic-number plasmas," D. Mosher, Phys. Rev. A **10**/6, 2330-5 (1974).

77. P. Bogen, in Plasma Diagnostics, W. Lochte-Hochgreven, ed., John Wiley & Sons, New York, p. 430 (1968).

78. "Electron energy distributions using the time-resolved free-bound spectra from coronal plasmas," D.L. Matthews, R.L. Kauffman, J.D. Kilkenny, and R.W. Lee, Appl. Phys. Lett. **44**(6), p. 586-8 (1984).

79. "Fast ions and hot electrons in the laser-plasma interaction," S.J. Gitomer, R.D. Jones, F. Begay, A.W. Ehler, J.G. Kephard, and R. Kristal, Phys. Fluids **29** (8), 2679-88 (1986).

80. D.V. Giovanielli, LAUR 76-2242; see also Ref. 32 of Gitomer, et al., Phys. Fluids **29** (8), 2670-87 (1986).

Table Captions

Table I. X-ray diode configuration and results.

Table II. X-ray spectrographic data, on a per-shot basis. J/shot and W/cm^2 column give laser quantities on target. C.F. gives conversion fraction of total x-rays into 4π sr (calculated as though isotropic) normalized to laser energy on target. Helium resonance line intensities were unfolded from neighboring satellites and intercombination line. For lower irradiance shots, the hydrogenic line intensities were too weak to measure reliably.

Figure Captions

Fig. 1 - Schematic diagram of the optical train of the Nd:glass laser system. (1) 90°retro mirror; (2) oscillator rod; (3) double aperture stop; (4) double plate polarizer; (5) aperture stop; (6) Pockels cell; (7) partially reflecting output mirror; (8) fluorescence radiation monitor (slow diode); (9) oscillator output monitor (fast diode, type MD1); (10) oscillator output calorimeter; (11) Pockels cell; (12) double plate polarizer; (13) beam expander; (14) first amplifier rod; (15) beam expander; (16) aperture stop; (17) second amplifier rod; (18) beam splitter; (19) output calorimeter; (20) output aperture stop; (21) laser output monitor (fast diode, type MD1); (22) turning prism; (23) to target chamber.

Fig. 2 - Schematic of the target chamber with associated laser-beam and x-ray emission diagnostics. The port at which the Seya-Namioka spectrograph was attached is indicated.

Fig. 3. - Laser diagnostics.
(a) The slow, fluorescence photodiode (50 μs/cm) monitored the normal laser rod fluorescence signature (1). The fast photodiode (2) shows the amplified Q-switched pulse as it appears at (21) in Fig. 1. The corresponding MD1 trace of the laser pulse at the target chamber is shown as (3), and the resultant x-ray trace from the Al-filtered PIN is (4).

(b) Under conditions of a slight laser-target interaction, the fluorescence (5) is abnormally enhanced prior to the Q-switch, and the output pulse is very low at the output diode (6) (see (21) in Fig. 1) and at the chamber (7); x-ray output is greatly diminished (8).

(c) P1/P2>2. Some of the shots displayed an unintentional second pulse following the main pulse by a fixed value ~100 nsec (recorded by a fast photodiode), produced by a reflection off the target. Shots with the main peak height exceeding the second peak height by at least 2 were admitted to the data set. The second pulse produces negligible x rays.

(d) P1/P2~1. A rejected shot displays a second pulse (recorded by the fast photodiode) comparable in height to the main pulse; x-ray production is still negligible.

Fig. 4 - Measured focal energy distribution at best focus on relative and absolute (W/cm^2) scales (left scales). The integral is given by the right-hand scale. The inset is a tracing of the regions of Bi evaporated by the laser pulse at various intensity levels.

Fig. 5 - Stereographic scanning electron micrographs of target craters from 3.2 J (top, shot 1527) and 32 J (bottom, shot 1523) pulses.

Fig. 6 - Pinhole camera images recorded at 1.5 x magnification from 32 J shots. Left: 25 μm pinhole, Kodak No-Screen film, shot 1523. Right: 1.15 mm aperture, Plus-X film, shot 1520.
Fig. 7a - PIN response functions for a hypothetical flat input spectrum. Response is the product of the x-ray transmission through the detector's light-tight window (upper curve, 40 μm Be and 19 μm mylar; lower curve, 38 μm Al), transmission through a 0.5 μm Si dead layer in the PIN, and the absorption in the 250 μm thick, fully depleted Si of the PIN. The small absorption edge feature at low energy is the Si K edge, which only shows on the more sensitive Be/mylar detector.

Fig. 7b - Variation of x-ray intensity with lens-target spacing.

Fig. 8 - Absolute K x-ray line spectra for 32 J, 15 J, and 7 J laser beams at best focus on an Al target.

Fig. 9 - Free-bound continuum above the He-like Al series limit (2086 eV) obtained at 32 J (shot 1571). The 1/e point on the ordinate represents 3.0×10^{13} eV/(sr-keV) or 4.8×10^{-6} J/(sr-keV). A few x-ray lines below 2086 eV are also plotted.

Fig. 10 - Laser-energy-dependence of absolute x-ray intensities, obtained with a Bragg spectrograph and with filtered silicon PIN detectors. The spectrographic data are corrected to give source emission, whereas the PIN data are as measured by the PIN in its location and with all of its filtration. The box at 13 J represents the spectrographic data, computationally folded into the Be/mylar PIN response function. Inset shows traces of the laser pulse and x-ray PIN for a typical shot.

Fig. 11 - Temperatures deduced from line ratios (Table II) and coronal model (X's). Single point (+) at 32 J on target gives temperature obtained from the slope of free-bound recombination continuum of Fig. 9.

Fig. 12 -

(Inset) Scope traces of the laser pulse (from the fast photodiode) and x-ray PIN. The intentional prepulse P1 precedes the main pulse P2 by a chosen amount >0.2 μs, and the peak height ratio P1/P2 is typically ~0.2. X-ray production occurs at the main pulse.

(Main figure) - Dependence of x-ray intensity versus spacing of the prepulse from the main pulse. The x-ray intensities measured by both PINs were normalized onto a single relative scale. The points for t = 0 had no prepulse. The inset contains tracings from an oscilloscope recording of the laser and x-ray intensities.

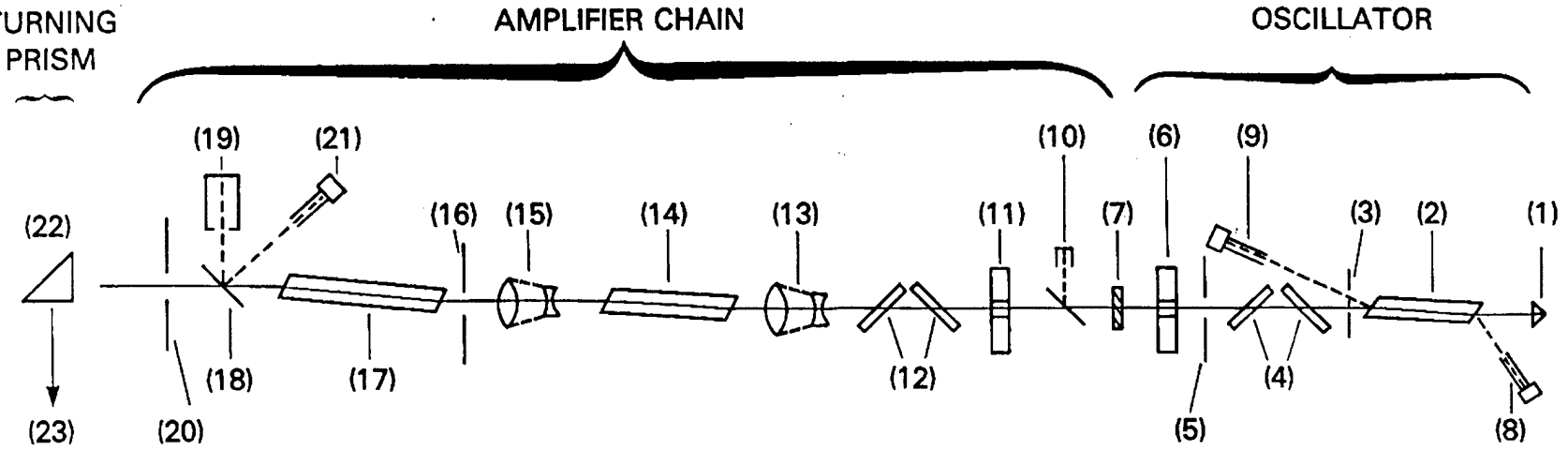

FROM NRL MR 3461

FIGURE 1

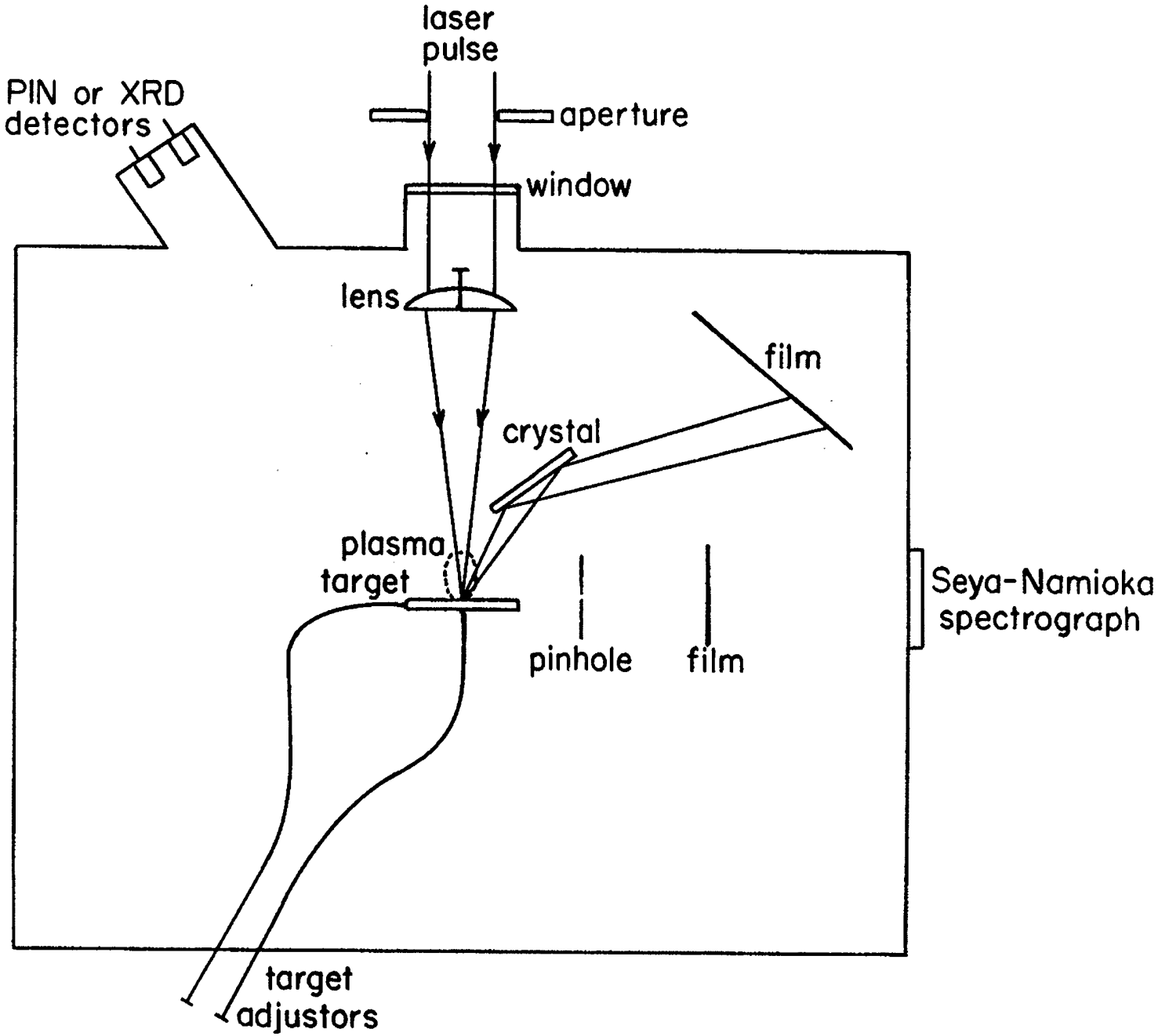
laser
pulse
PIN or XRD
detectors
aperture
window
lens
film
crystal
plasma
target
pinhole
film
Seya-Namioka
spectrograph
target
adjustors

FIGURE 2

FIGURE 3a

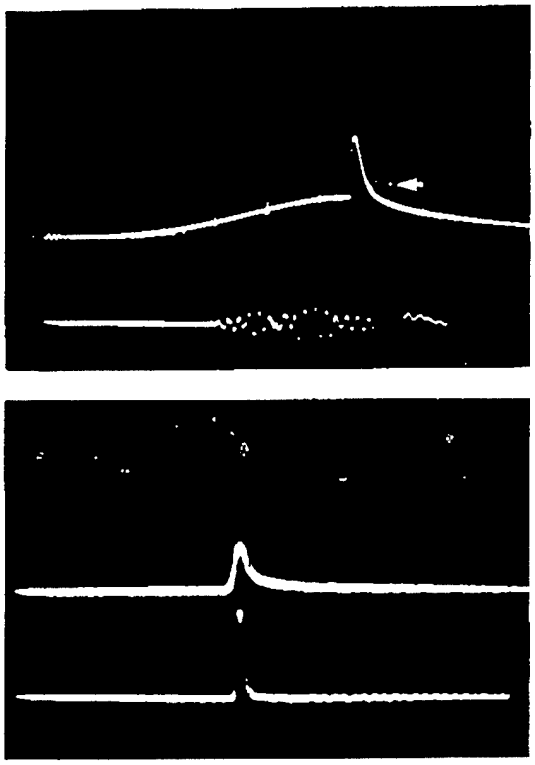

FIGURE 3b

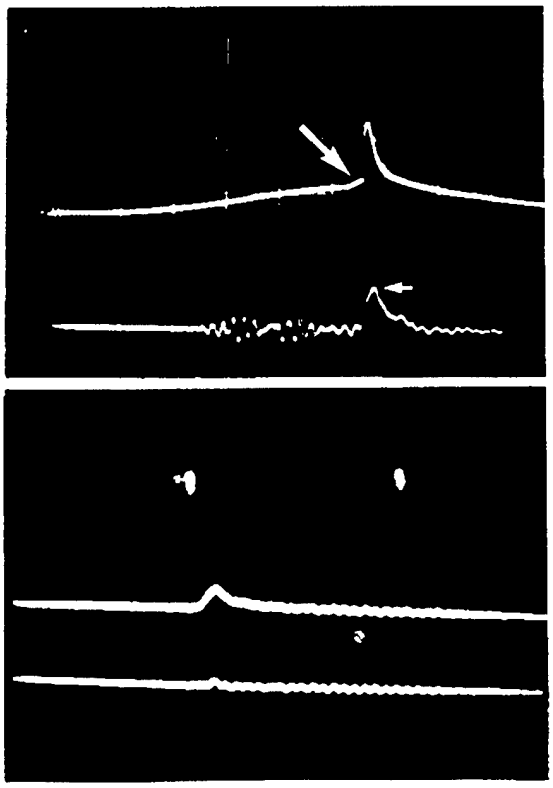

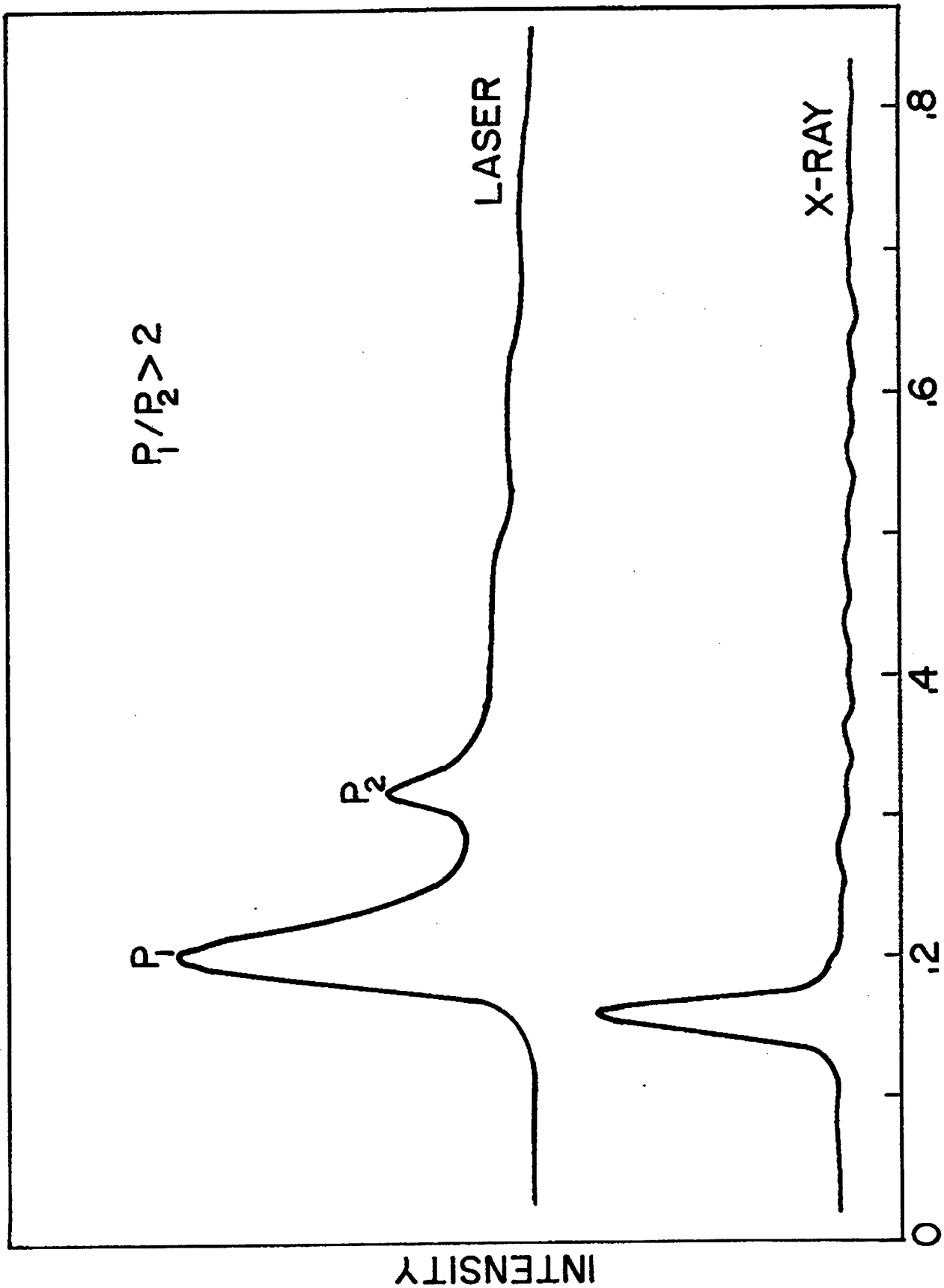

FIGURE 3c

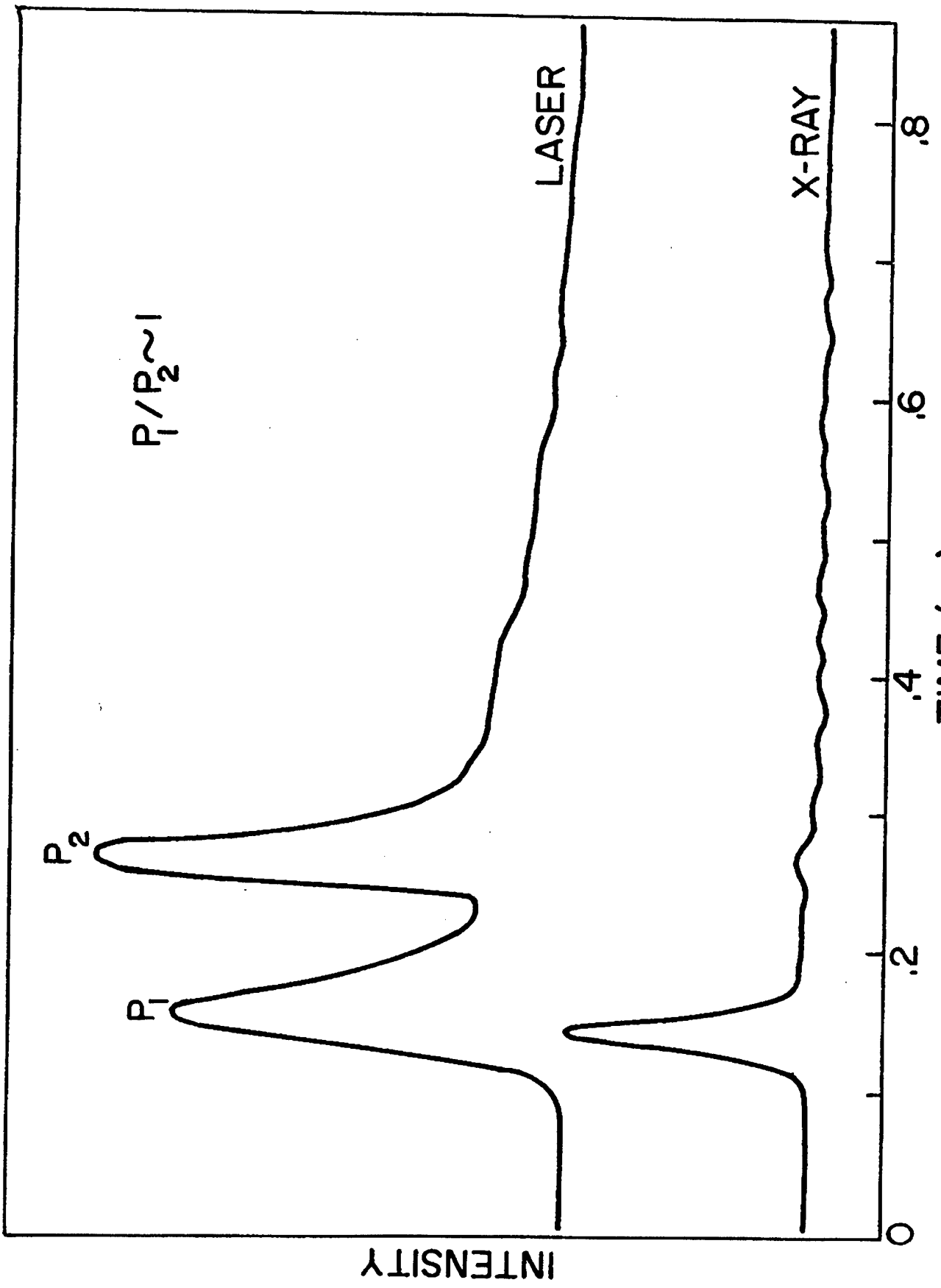

FIGURE 3d

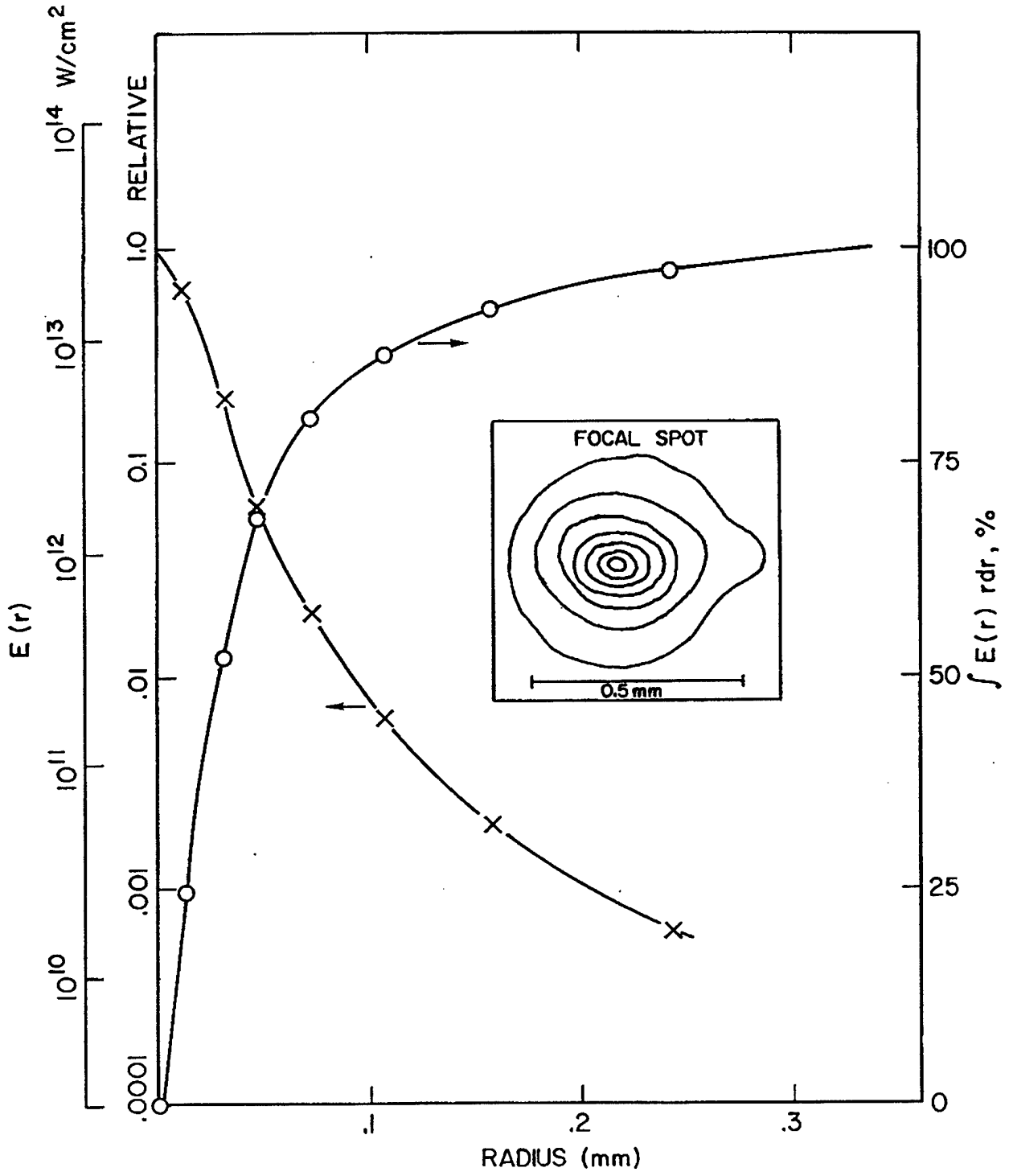
10^{14} W/cm^2
1.0 RELATIVE
0.1
.01
.001
.0001
10^{13}
10^{12}
10^{11}
10^{10}
E (r)
100
75
50
25
0
$\int E(r)\, rdr$, %
FOCAL SPOT
0.5 mm
.1
.2
.3
RADIUS (mm)

FIGURE 4

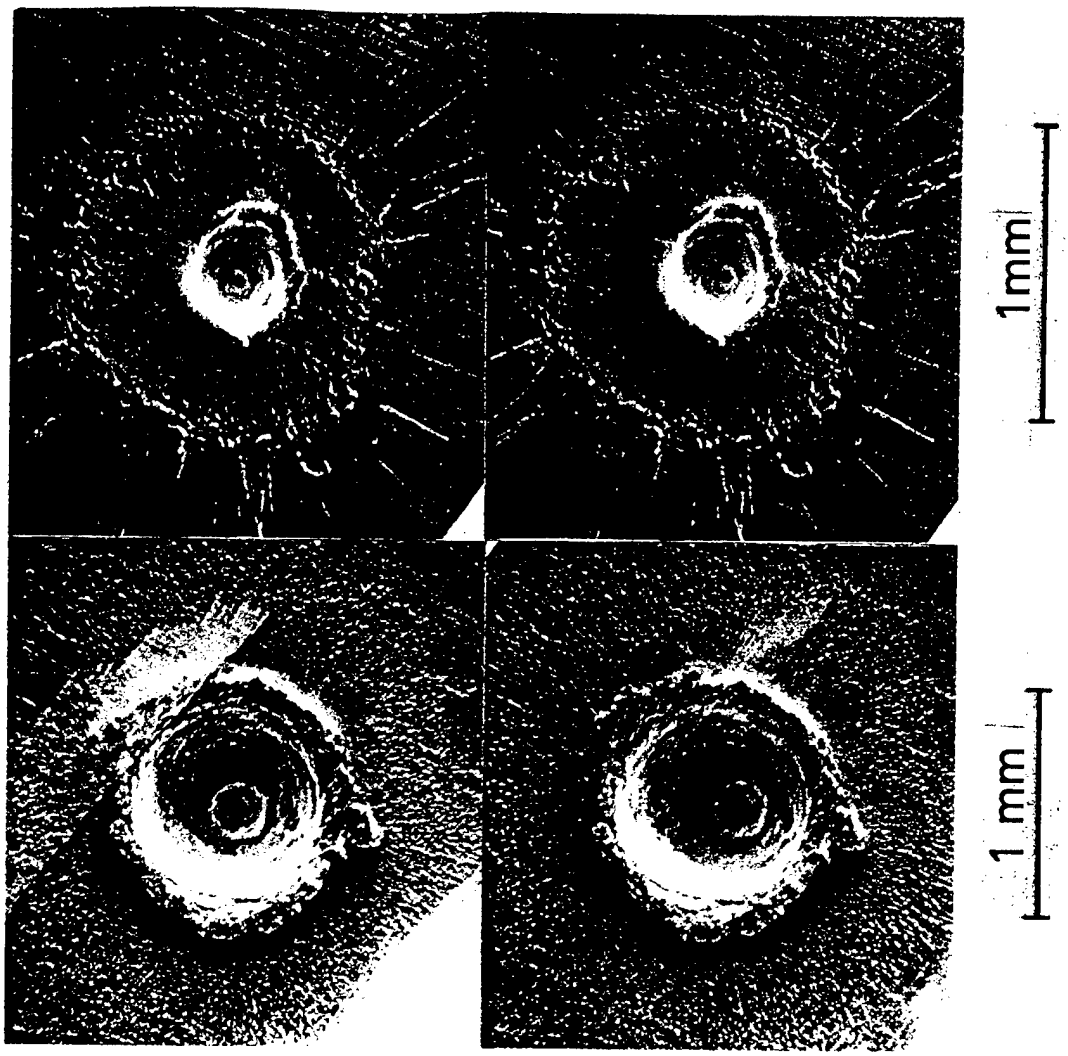

FIGURE 5

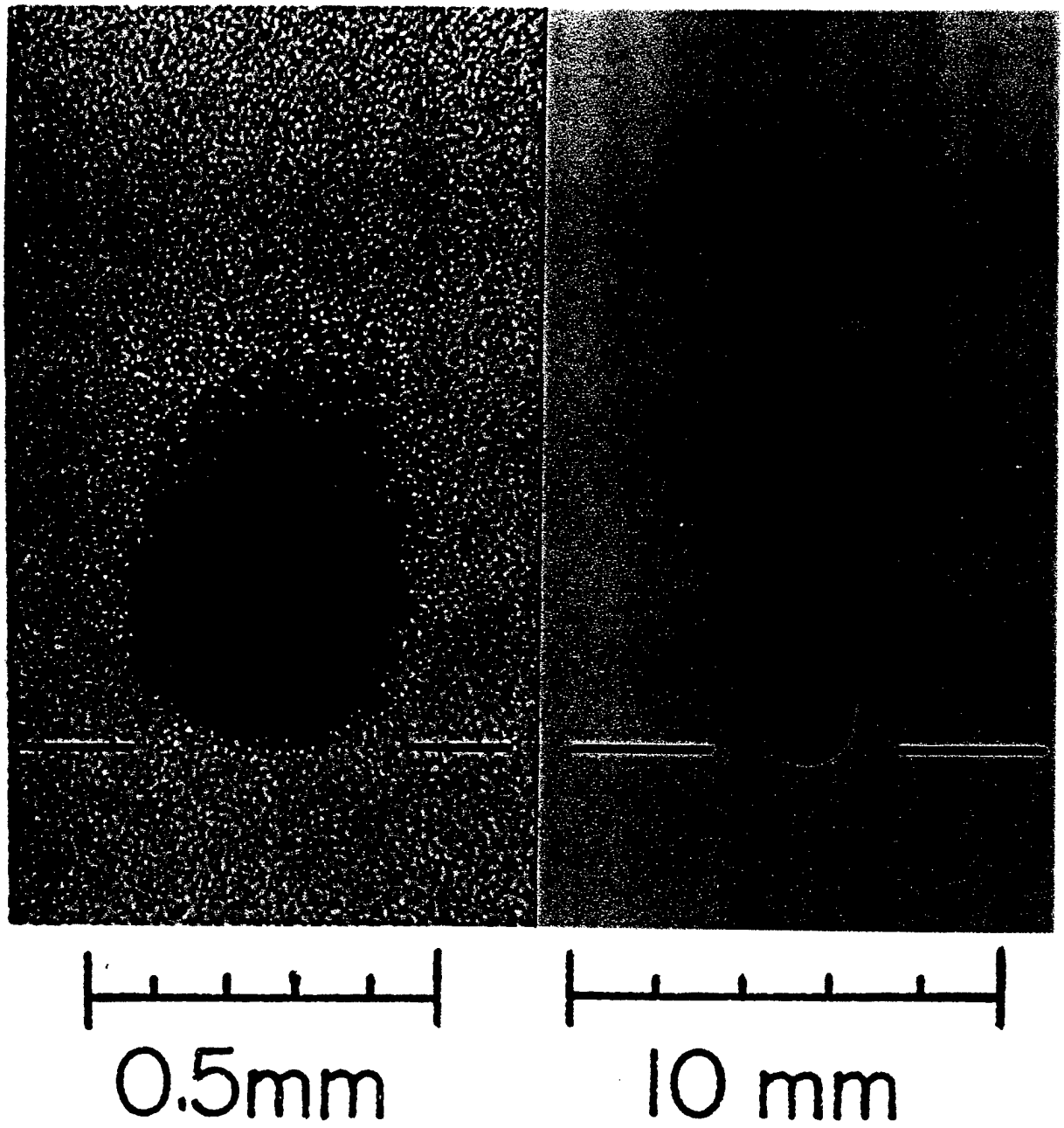

FIGURE 6

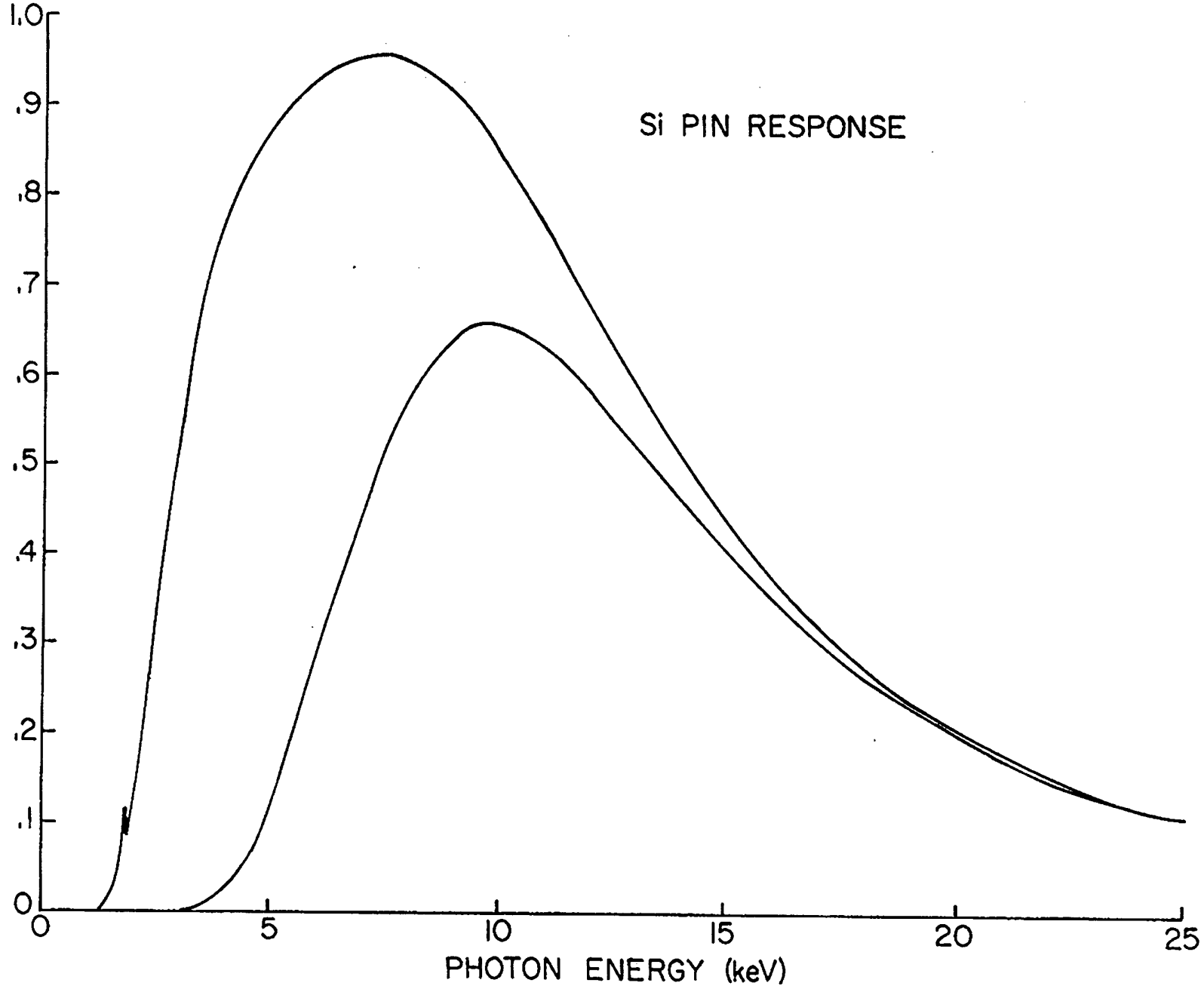
Si PIN RESPONSE
1.0
.9
.8
.7
.6
.5
.4
.3
.2
.1
0
0
5
10
15
20
25
PHOTON ENERGY (keV)

FIGURE 7a

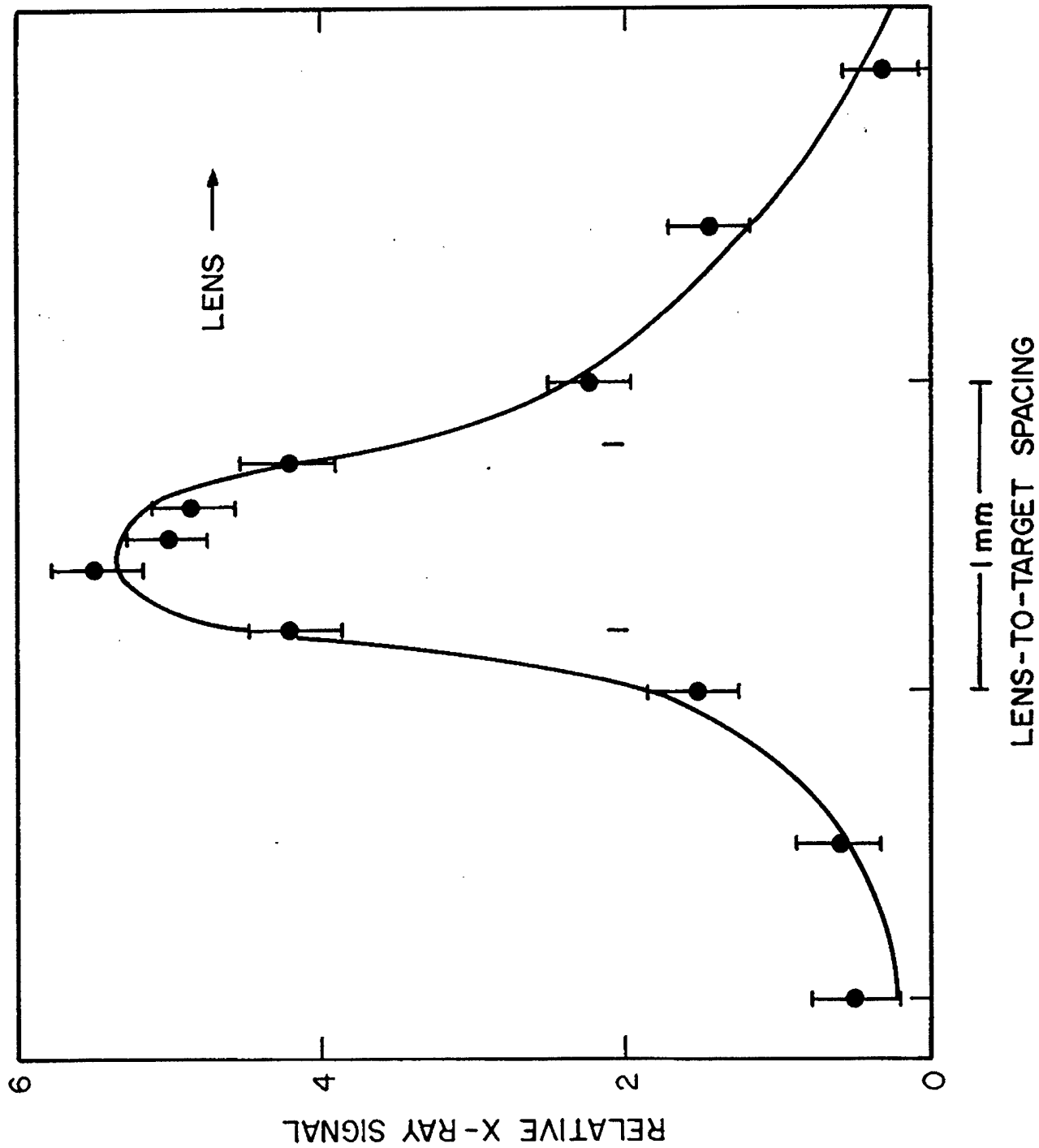

FIGURE 7b

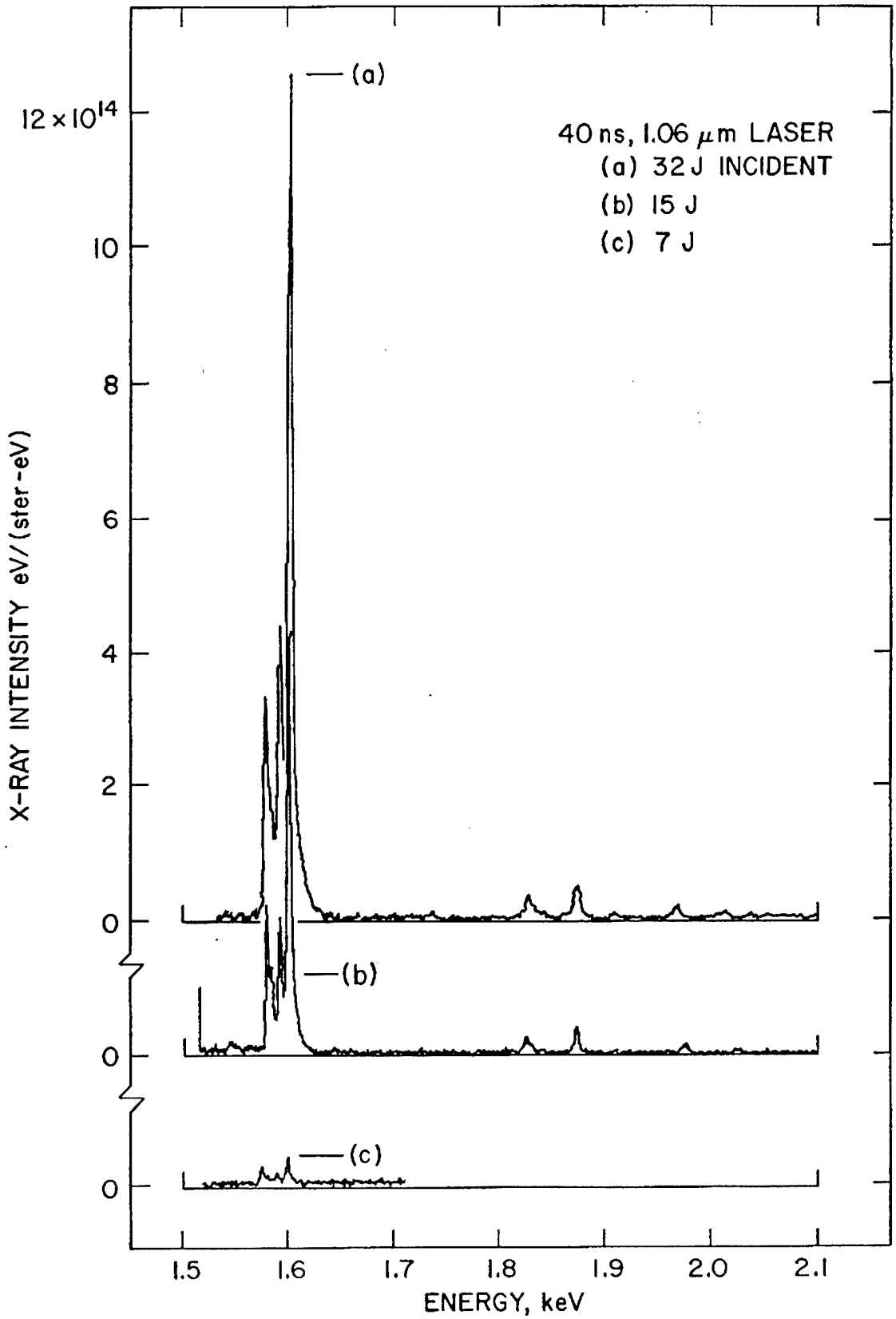
40 ns, 1.06 μm LASER
(a) 32 J INCIDENT
(b) 15 J
(c) 7 J
(a)
(b)
(c)
12 × 10^14
10
8
6
4
2
0
0
0
X-RAY INTENSITY eV/(ster-eV)
1.5
1.6
1.7
1.8
1.9
2.0
2.1
ENERGY, keV

FIGURE 8

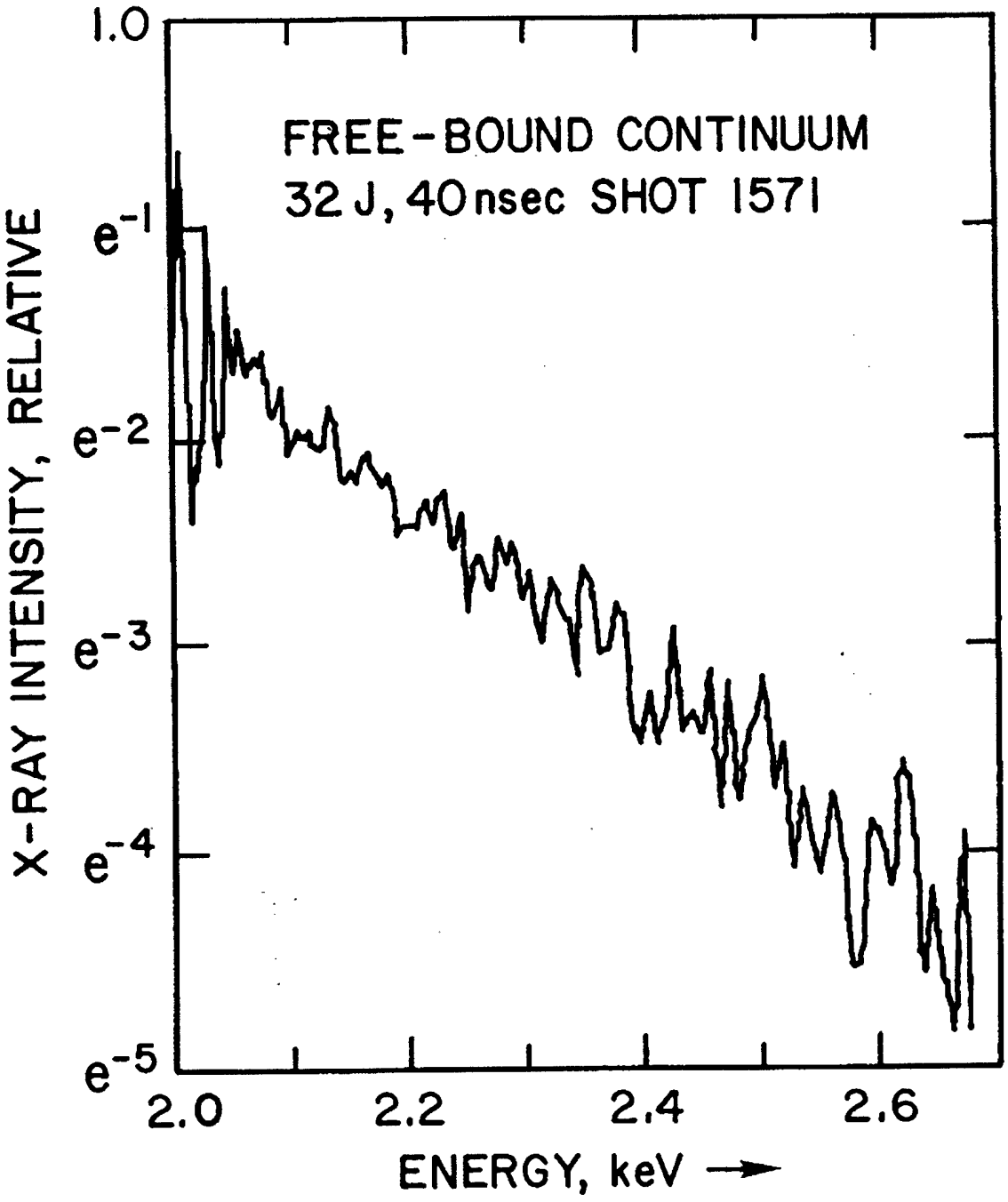
FREE-BOUND CONTINUUM
32 J, 40 nsec SHOT 1571
X-RAY INTENSITY, RELATIVE
1.0
e-1
e-2
e-3
e-4
e-5
2.0
2.2
2.4
2.6
ENERGY, keV

FIGURE 9

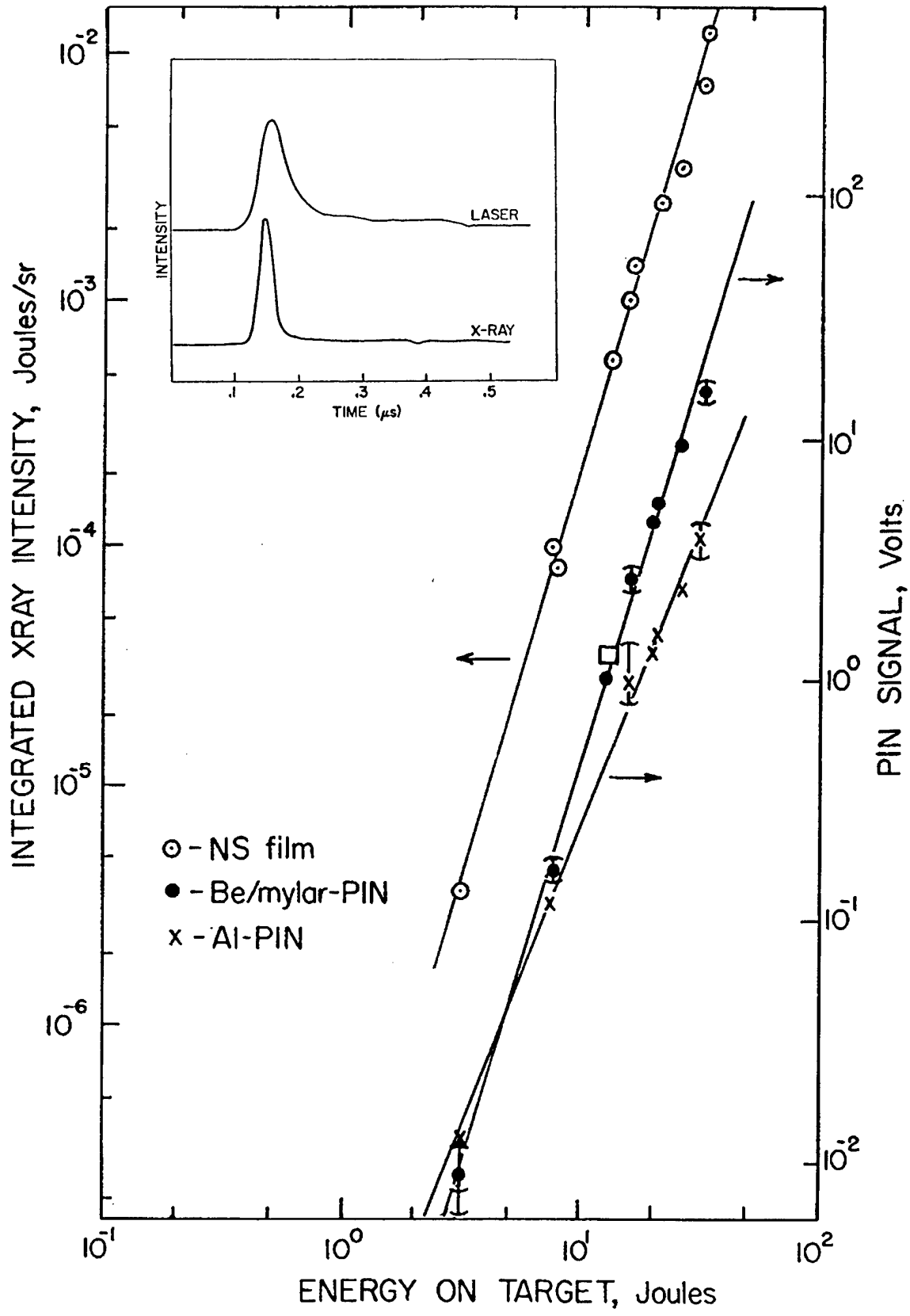
INTEGRATED XRAY INTENSITY, Joules/sr
PIN SIGNAL, Volts
ENERGY ON TARGET, Joules
INTENSITY
LASER
X-RAY
TIME (μs)
⊙ - NS film
● - Be/mylar-PIN
x - Al-PIN

FIGURE 10

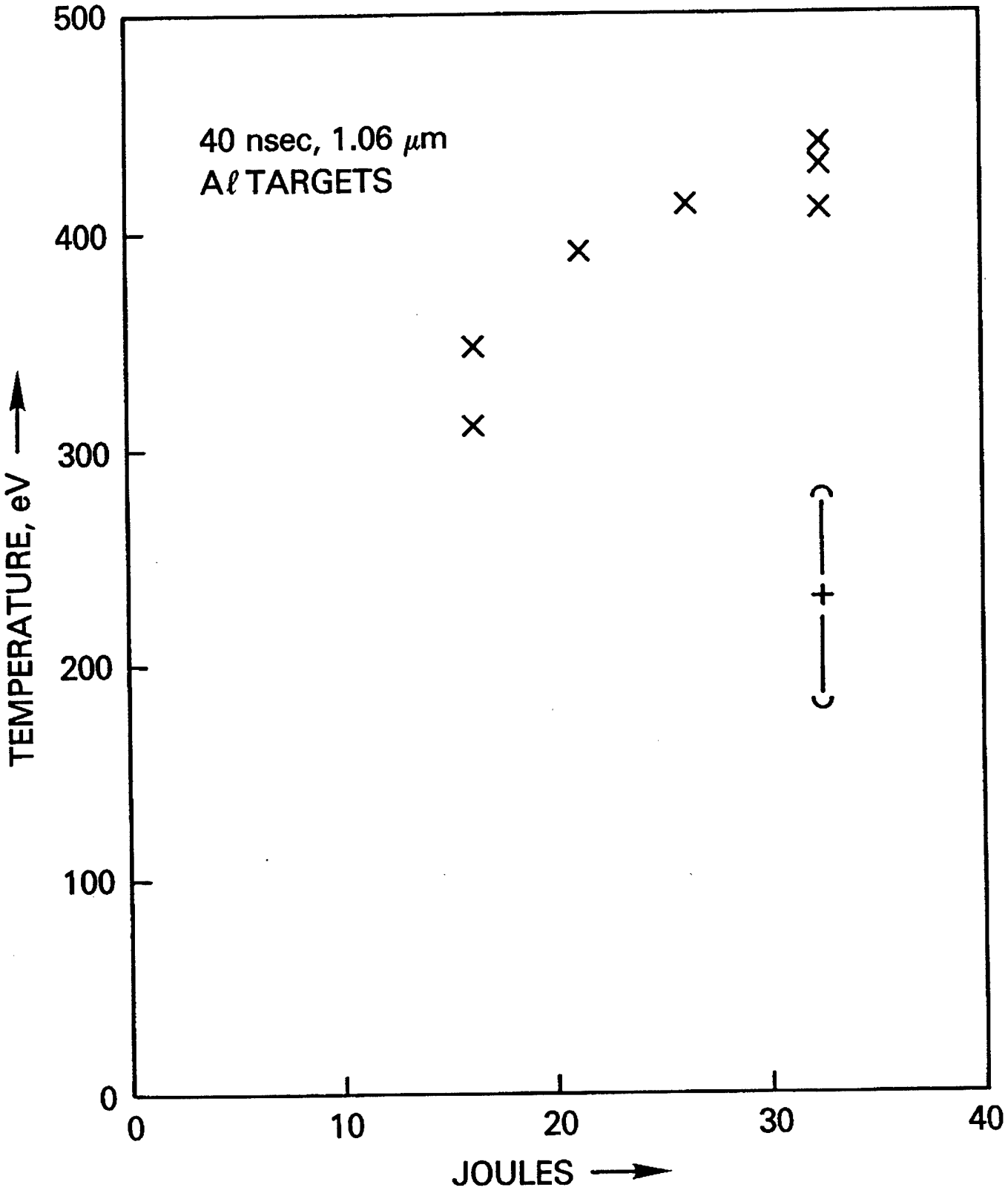
40 nsec, 1.06 μm
Aℓ TARGETS
TEMPERATURE, eV
JOULES
500
400
300
200
100
0
0
10
20
30
40

FIGURE 11

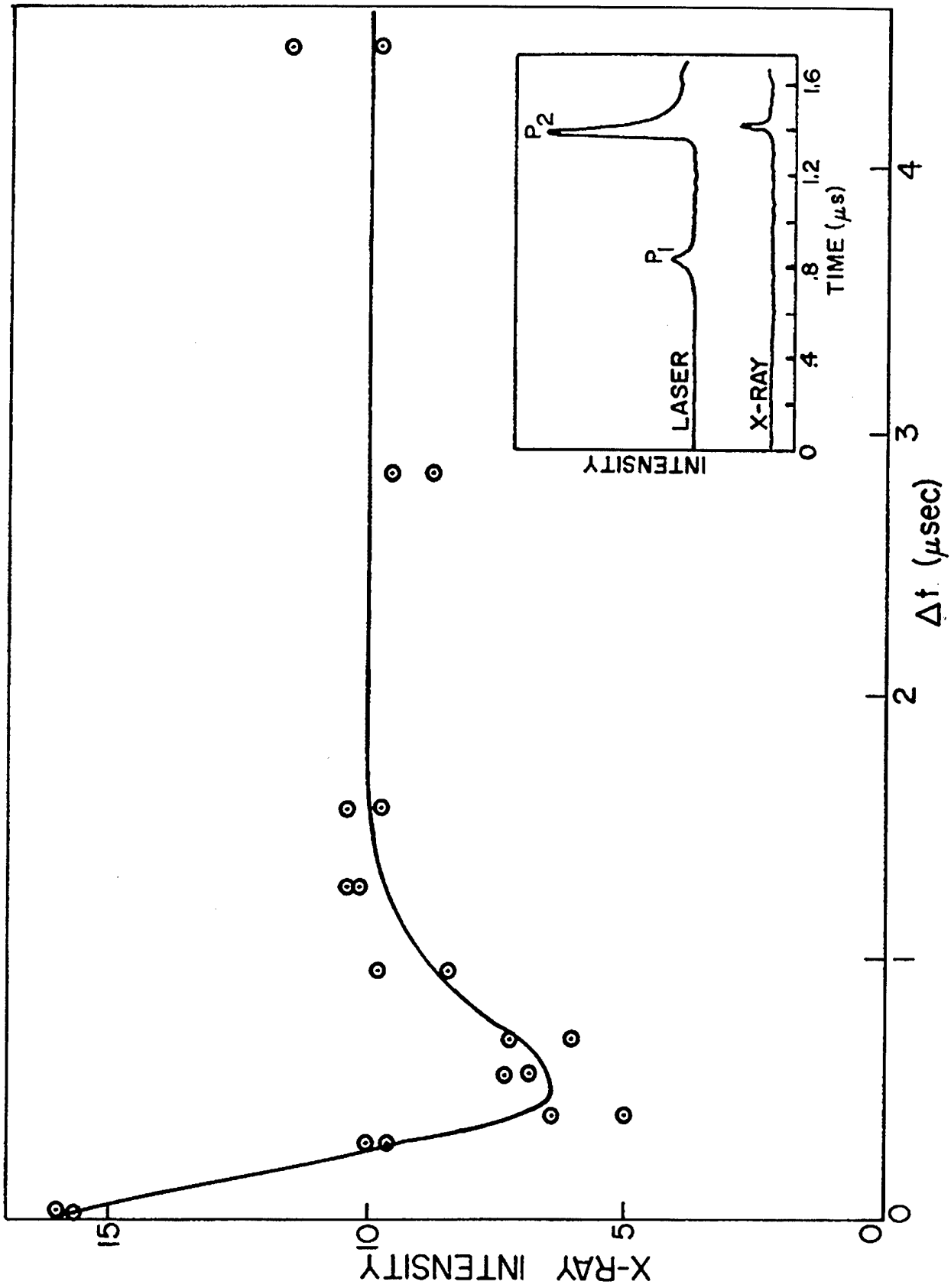
X-RAY INTENSITY
15
10
5
0
0
1
2
3
4
Δt (μsec)
INTENSITY
LASER
X-RAY
P1
P2
0
.4
.8
1.2
1.6
TIME (μs)

FIGURE 12